Master Thesis

September 12, 2019

# Hybrid Storage System coupled with PV Power Plant for Primary Frequency Control

**MSc SELECT: Environomical Pathways for Sustainable Energy Systems**

**Author:** Alberto Danese

**Supervisor:** Francisco Díaz-González

This page was intentionally left blank.

*Service to others is the rent you pay for your room here on Earth.*

(Muhammad Ali)

*Avoiding climate breakdown will require cathedral thinking. We must lay the foundation while we may not know exactly how to build the ceiling.*

(Greta Thunberg)

## Abstract

Transitioning from fossil fuel classical generators to intermittent, non-synchronous sources like solar and wind presents a series of technical challenges to be overcome on large scale. A specific issue is related with the concept of inertia of the electrical system: the less the number of generators with rotating masses connected to the grid, the less the value of total inertia of the system.

Solar driven generating units such as PV present no mechanical inertia, therefore their increase in the electricity generation mix decreases the total inertia of the system, which lower the overall reliability of the system. Logically, it is of fundamental importance to ensure that PV power plants are more and more capable to provide ancillary services to improve the stability of the grid, especially in terms of frequency. The need for faster frequency regulation and voltage control in the electrical system can be ensured effectively by energy storage systems. In the purpose of this study it is addressed the possibility of large battery systems to overcome the variability of the solar resource, and the forecasting error, resulting in higher profit for a PV plant operator.

The methodology consists in the formulation and the resolution of a Non-Linear Programming (NLP) problem, implemented in GAMS, applied to a 9.4 MW PV power plant. The output of the simulation determines the parameters that characterize the optimal Hybrid Storage System, in order to increase the profit during one typical day of solar radiation (01 April), while participating actively in the PFC. The result of the investigation determines that the most profitable hybrid storage system to be coupled with the PVPP is formed by a 883 kWh Lithium Ion Battery and a 32 kWh High Speed Flywheel. The analysis is finally complemented with a realistic simulation in Simulink environment in which is developed and implemented a prototype of EMS.

# Contents

## List of Figures

## List of Tables

**Acronyms**

The following acronyms are used in this manuscript:

| | |
|---|---|
| AC | Air Conditioning |
| BMS | Battery Management System |
| DMP | Daily Market Price |
| EMS | Energy Management System |
| ESS | Energy Storage System |
| EV | Electrical Vehicles |
| FESS | Flywheel Energy Storage System |
| HESS | Hybrid Energy Storage System |
| HSS | Hybrid Energy Storage System |
| SoC | State of Charge |
| SoH | State of Health |
| PFC | Primary Frequency Control |
| PVPP | PhotoVoltaic Power Plant |

# 1 Introduction

The recent publication of the Intergovernmental Panel on Climate Change on the impacts of global warming of 1.5 °C above pre-industrial levels [1] raised the attention towards fast transition of the entire energy system towards zero emission. Decarbonization of the electricity sector through energy sources is only part of the solution to achieve this ambitious plan: no zero-carbon emission scenario can be reached without implementing substantial change in the way society produce goods, transport things and people, consume energy and design homes [2].

From a technical point of view, inter-connection of electrical systems, demand-side response and decentralization of energy sources must all play a role in the transition of the global electrical architecture. Finally, analyzing recent predictions based on 100% renewable energy system in 2050, PV power plants represent the technology that will cover the highest share of electricity supply across the world [3].

The scope of the thesis is to investigate how hybrid storage solutions can cooperate together with large solar power plants, in order to comply with recent regulations on Primary Frequency Control, while providing ancillary services and increase economic profit through a more intelligent use of the solar resource.

## 1.1 Research area

The business applications in which a battery can be exploited are different and for different actors. Distribution grid operators can make use of mid-scale batteries for power quality and reliability services, resulting in postponing or avoiding structural network upgrades [4]. Thanks to the increasing affordability of storage devices, also households, especially the ones who own a PV system, choose to maximize self-consumption trough small-scale batteries [5].

At the utility level, storage solutions increase their flexibility to operate within energy markets, gain from arbitrage and ancillary services [6]. Moreover, renewable power plants can benefit from the smoothing effect provided by storage systems ensuring they always comply with regulations such as Active Power Ramp Rate. Specifically, in case of PVPP, ramp rate control is usually provided through a moving average method that gradually change of output active power of the PV inverter [7]. The

main advantage of coupling an Energy Storage System in this case ,is that losses can be stored when the power is increasing rapidly, while less reserve has to be curtailed in period of drastic energy output reduction.

Nevertheless, the effective integration of conventional storage devices in the energy system is hindered by economic and technological issues. Although the capital costs of storage devices has seen a steep decrease in the last decade [4], its cost is still significant compared to the capital of the PV power plant [8]. The minimization of the battery capacity represents one of the main instrument to decrease the capital cost of the ESS. Many different minimization objectives can be used in order to set the capacity of the battery: from technical requirements such as power fluctuations minimization to overall profitability. Hybridization of different storage technologies can be a cost-effective solution in order to minimize capital costs, maximizing profit and achieve technical requirements such as technological lifetime or primary frequency control regulations.

### 1.2 State of the Art

One of the most attractive services for a large-scale battery operator is without doubts primary frequency control (ancillary service) and arbitrage (bulk energy service). While PFC results to be one of the most lucrative application of large batteries in European markets where this service is paid [9], arbitrage is highly dependent on the daily market price trend, therefore the revenue stream is difficult to predict on a long term time range. Nevertheless [10] demonstrates that increased profits can be achieved optimizing the dispatch planning for German intra-day market on 15 and 60 minutes range. On the other hand, several papers investigated the possibility to increase the revenue stream in the use of storage devices operating in multiple markets: in particular [11] explores the increase in revenue stream adding on top of arbitrage service alternative sources such as the reserve services in the UK electrical market. These papers assess the economic revenue from the use of the storage system alone, without investigating the added benefits from coupling the battery with a large scale PV Power Plant.

In [12] these benefits are taken in account calculating the revenues change on annual basis from the improved generation, peak power generation, and reduced line losses, while accounting for storage costs. Moreover the analysis output is compared for two different battery chemistries to further corroborate the model feasibility. In [13] the main goal is to achieve a smoothing strategy through the

use of a Hybrid Storage System (composed of a vanadium redox battery and a supercapacitor bank). A statistical approach is used to properly size the batteries and ensure that the HSS is most of the time capable of ensuring the smoothing effect on power ouput fluctuations. Main limits of the study are the low input data resolution (every 30 mins) and no reference to economic benefit. Data resolution is central in case frequency control has to be ensured and simulated, therefore lower time step is required.

Instead in [14] a grid-connected microgrid is considered, with 1-minute resolution data and a HSS coupled with PV power plant in order to decrease the reliance on grid input energy. Flywheel has been considered in order to decrease high current to be discharged from the battery, limiting the stress on the battery itself resulting in a significant increase in storage expected lifetime estimated through a post-processing Rainflow algorithm.

### 1.3 Objectives and Expected Outcomes

The contribution of this study is to investigate the possibility for HESS to be coupled with grid-connected PVPP for primary frequency control and the forecasting error minimization. Sizing and operational optimization take as model the approach contemplated in [15], adding complexity to the GAMS model with the introduction of a second storage device as in [14]. Given the limitations of optimization processes, in which is difficult to implement an algorithm like the Rainflow [16], it is therefore investigated a way to include a simple but effective Degradation model (in Section 4) in the optimization process. The Operational Strategy resulting from the first phase is post-processed in order to highlight Operational guidelines for the EMS. Moreover, the result obtained from the optimization is further developed through an accurate model, that simulates time-responses. In this way the EMS takes in account the physical model and the capabilities of the battery while ensuring the best operational strategy. In the opinion of the author, the expected outcome should highlight an economic benefit from the implementation of the HESS. In fact, hybridization results in an increase of profits while keeping the investment costs lower: a small storage device, such as the flywheel, is supposed to provide high power ratings for relatively low overall cost, while a large battery can ensure the energy capacity is provided when a large under-frequency deviation arises. The operational strategy, and consequently the EMS should activate the storage devices depending on their different capabilities (especially time-response and SoC) and their respective degradation calculated costs.

### 1.4 Structure of the Research

The research will focus on hybrid storage solution that can be complemented to the PVPP to successfully comply with UK Primary Band Control and European Grid Code. The investigation is articulated in different steps:

- Section 2: Grid code and economic Framework for Primary Frequency Control;
- Section 3: the technology chosen is briefly presented;
- Section 4: it is discussed the topic of aging models for Lithium Ion batteries and are presented two simple methods to account for the calendrical degradation of the battery in the optimization phase;
- Section 5: solution is modelled in an optimization environment, where input from the techno-economic analysis are used to quantify the economic return of the implementation in a real electricity market process.
- Section 6: results from GAMS optimization are shown highlighting main results and developing a partial sensitivity analysis.
- Section 7 the storage model obtained is finally simulated taking in account more technical constraints, ensuring the best economic operational strategy while preventing the battery from being stressed resulting in a contraction of its technological lifetime.
- Section 8: project budget and environmental impact estimation.
- Section 9: conclusions and future work.

# 2 Economical and Regulatory Framework

Electricity markets were in the past tailored for large scale, centralized power plants that supplied electricity with low intermittence and relatively low forecasting error. Considering the present and future transition of the energy system, market regulation developments are key in order to unlock the economical possibilities for storage technologies and renewable generation. On this regarding, it is useful to depict an overview on Frequency containment reserve regulations and indications at a European level (ENTSO-E), but at the same time quantify the revenue stream with a specific national market. Therefore the Spanish and the UK grid codes are analyzed, evaluating which is more suitable and economically proficient for the scope of the project.
It must be highlighted that terminology currently in use to designate different type of reserves may vary across different network codes:

- Frequency Containment Reserves (in UK Primary Band Control) referred as Primary Reserve;
- Frequency Restoration Reserves referred as Secondary Reserve;
- Replacement Reserves referred as Tertiary Reserve.

## 2.1 ENTSO-E Regulatory Framework

### 2.1.1 Frequency Containment Reserve

**Definition**

From Article 3(2)(6) of the EU Network Code on System Operation FCR is defined as "the active power reserves available to contain system frequency after the occurrence of an imbalance". This category typically includes operating reserves with activation time "up to 30 second" and are usually activated automatically and locally. When the time limit is reached, and if the deviation is still in place, FCRs are substituted by Frequency Restoration Reserves [17].

**Market information**

Each TSO shall determine the imbalance price for:

- each imbalance settlement period;

- its imbalance price areas;
- each imbalance direction.

The payment of the activated volume of balancing energy for the frequency containment process shall be defined as described in Article 55 of the Commission Regulation (EU) 2017/2195 of 23 November 2017 depending on the imbalance direction as in Table 1.

| | Balancing energy price positive | Balancing energy price negative |
|---|---|---|
| Positive balancing energy | Payment from TSO to BRP | Payment from BRP to TSO |
| Negative balancing energy | Payment from BRP to TSO | Payment from TSO to BRP |

Table 1: Payment for frequency containment process

The imbalance price for positive imbalance shall not be greater than, alternatively:

- the weighted average price for negative activated balancing energy from frequency restoration reserves and replacement reserves;
- In the event that no activation of balancing energy in either direction has occurred during the imbalance settlement period, the value of the avoided activation of balancing energy from frequency restoration reserves or replacement reserves.

### 2.1.2 Frequency Restoration Reserves

**Definition**

These reserves are defined as active power reserves available to restore system frequency to the nominal frequency with an activation time typically between 30 seconds up to 15 minutes (depending on the specific requirements of the synchronous area) [18] . FRR can be distinguished between reserves with automatic activation (aFRR) and reserves with manual activation (mFRR).

**Market Information**

On the official website of ENTSO-e is reported that the average price for the FRR has "commercially sensitive interconnection with the imbalance price" [18] but no other indication is given on this pur-

pose.

## 2.2 Spanish Regulatory Framework

### 2.2.1 Primary Band Control

Red Electrica Espana does not include this service as an ancillary one: in fact the primary reserve is mandatory and not paid. According with the Union for the Coordination of the Transmission of Electricity (UCTE), each generating unit has to provide an upward reserve to be used for downward frequency drops: the reserve magnitude varies between 1.5% to 10% of the active power produced [19]. It is important to highlight that, for current regulations, the time period in which the service is required correspond to the period of the day in which the PVPP is actively producing power.

Every time step presents a frequency deviation value from 50Hz, therefore the generating unit is forced to curtail or increase the energy output by an energy amount: this value can be calculated following frequency control droop established by the ENTSO-E, following limits and constrains instituted by the Spanish Grid Code.

The result is summarized in Table 2

Table 2: Primary Frequency Control Regulation.

| $\Delta f$ | $\Delta P(t)/P(t)$ | Comments |
|---|---|---|
| $\leq -\Delta f_{max}$ | 0.1 | Supply of 10% of the available power |
| $\geq -\Delta f_{max} \wedge \leq -0.02$ | Following chosen slope | ENTSO - E usually sets to 5 % |
| $\geq -0.02 \wedge \leq +0.02$ | 0 | Dead Band: no reserve provision |
| $\geq +0.02 \wedge \leq \Delta f_{max}$ | Following chosen slope | - |
| $\geq \Delta f_{max}$ | 0.1 | Curtailment of 10% of the available power |

Current regulations moreover does not regulate the maximum frequency drop or increase ($\Delta f_{max}$), that can be chosen depending on the Inverter capabilities and other factors. For the purpose of this study $\Delta f_{max} = 0.5$.

As most of European regulators (Ireland, Germany...) the minimum capability of actuation of primary

reserve is 15 minutes [20].

### 2.2.2 Secondary Band Control

The scope of this band control is to maintain generation-demand balance correcting deviations lasting more than 20 seconds up to 15 minutes. This service is remunerated by means of market mechanisms via two concepts: availability (control band) and usage (energy). The regulation deviation is measured by the TSO and the requirements for each regulation is distributed every four seconds [21].

**Mechanism of action**

After the upward reserve market is closed, the SO procures FRR capacity for each of the 24 hours of the day-ahead. Generators committed in this market receive the marginal price of the market (in €/MWh) for the capacity and an energy price (in €/MWh) in case the SO activates FRR. "This energy price is given by the marginal price of the RR energy that would be required to replace the activated FRR according to the Replacement Reserves energy bid ladder" [22].

### 2.2.3 Forecasting Error

If the utility is not able to supply the contracted energy in the DA market (not even throgh intra-day transactions), this kind of market is activated to penalize generation errors. The Figure 1 summarize the compensation scheme that penalize or reward errors depending on the system necessity.

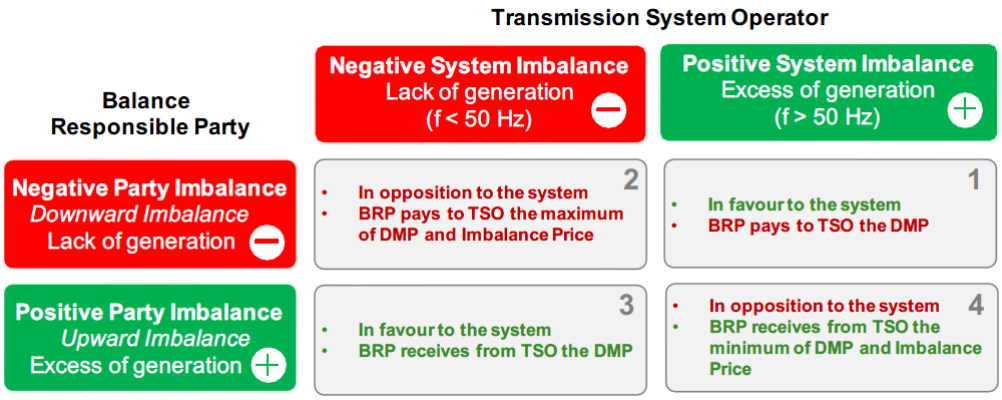


Figure 1: Spanish imbalance prices according to different system and Generating unit circumstances [23]

#### 2.2.4 Diversion Management Market

This market is activated if the SO measures a loss in the energy delivered by producers larger than 300MW. It covers the period between intra-day market sessions, participation is optional, and allocation is assigned on an economic merit order basis.

### 2.3 UK Regulatory Framework

#### 2.3.1 Primary Band Control

According to the European legislation, the primary reserve is a service that should be paid as a result of the imbalance direction and the volume of energy provided during the deviation.
To better assess the revenue possibility offered by the primary reserve control and properly size the storage system, it is investigate the UK electrical regulation. The british Electrical System Operator (ESO) provides an accurate payment mechanism for the frequency control.
Frequency services are mandatory for large generators (for national grid $> 100MW$), but suppliers are remunerated for the volume of energy supplied (£/MWh) and the availability (£/h).

**Definition**
The analysis focus on a PV Power Plant of 9.4MW, therefore the primary frequency control is not mandatory and is regulated by the market mechanism called "Firm Frequency Response". Here the main requirements:

- deliver minimum 1MW response energy;
- have suitable operational metering;
- pass the FFR pre-qualification assessment [24];

**Market Information**
Response represents the ability to modify generation or demand to compensate for changes in system frequency within 2-30 seconds, depending on FFR service type. The FFR service is split into two physical products, Non-Dynamic (static) and Dynamic frequency response. There are three main Dynamic service types: primary, secondary and high. Figure 2 shows the response speed and length

of response. Primary and secondary response are employed for negative frequency deviation, while the high frequency response refers to positive frequency deviations.

| FFR product type | | Response speed | Length of response |
|---|---|---|---|
| Non-Dynamic – Secondary response is the only Non-Dynamic response currently procured. | | Within 30 secs | 30 mins |
| Dynamic – A Dynamic service can provide Primary, Secondary and High response, or Primary and Secondary only or High only. | Primary | Response required within 2 secs, with full response by 10 secs. | 20 secs |
| | Secondary | Within 30 secs | 30 mins |
| | High | Within 10 secs | Indefinitely unless otherwise agreed. |

Figure 2: Firm Frequency Response overview

The compensation is calculated hourly, as in Equation 1

$$\lambda_{UFR}(\mathrm{h}) = \lambda_M(\mathrm{h}) \cdot 1.25 \tag{1}$$

The availability fee has been extracted from an historical tender data where a battery energy storage system of 2.4 MW has been nominated for FFR [25]. The fee is quantified to be 42 £/h, using the monetary change at the 3.05.2019 1.17€/£ the availability fee is $\lambda_{av} = 20.48$ [€/$MW$] for every hour of availability.

**Conclusion**

From the analysis of the Spanish and UK market regulations is assessed that UK code is more promising for the quantification of the revenue stream. In particular it is investigated how the Dynamic service can increase the profits of the PVPP owner.

# 3 Techno-Economical Analysis

## 3.1 Primary Battery

For the purpose of the study high quality Lithium-Ion batteries are decided to be implemented as primary battery, being more suitable for fast regulating primary frequency control than low cost Lead Acid: sudden changes in current rate can lead to temperature increase of the storage, decreasing significantly the SoH of this type of batteries [26]. Lithium Ion is a proven technology for Primary Frequency Control on large scale: in fact all large scale BSS projects until late 2018 in Germany use Lithium Ion Technology [27]. On the other hand, flow battery technology has been considered but this choice was discarded because the experience from field test is relatively low [28].

## 3.2 Lithium Ion Technology

Lithium-Ion family of batteries hosts a wide range of different chemistries: the battery performance characteristic varies significantly through the different types. The most common electrolyte used is typically a liquid organic solvent mix with dissolved lithium salts (like Manganese, Phosphate...). The main drawback of this technology is the higher specific cost, if compared with Lead Acid, but superior technical qualities make this technology more reliable under stress conditions.

Common characteristics are low self-discharge, high-rate and high-power discharge capability, excellent round-trip efficiency, a relatively long lifetime and a high energy density [29]. The latter although is not particularly interesting for stationary application where the weight is not a critical parameter as in EV's applications.

Some drawbacks are instead the higher upfront cost and thermal stability: once the battery cell overpasses the so-called "runaway point" (around 67 °C), the cell may catch fire. A thermal management system constrains the charging current to an upper bound in order to prevent these types of faults, resulting in higher control complexity. In fact, the BMS system of a Lithium Battery is generally more elaborated than a Lead acid battery. Moreover, another parameter that drives up the cost of Lithium technology is the presence of Cobalt and nevertheless this adds a human cost as well [30].

### 3.3 Secondary Battery

Following as a model the solution developed by [14] the secondary battery is decided to be a flywheel. This technology presents a high cycle life, long operational life and high round-trip efficiency (>85%). Industrial producers have tested and proven these high quality characteristics over several projects [31]. Moreover technology is characterized by an overall low environmental impact [32]. Finally, FESSs are demonstrated to be suitable for producing and be charged by medium and high powers (kW to MW) during short time-periods (seconds) [33] making them a good candidate to ensure fast PFC.

### 3.4 Flywheel

One of the most important characteristic of this technology is the velocity at which the device is able to rotate without overcoming the maximum tensile strength. This last factor characterizes the capacity of the flywheel to withstand centrifugal forces acting on the disc and can be calculated by different and complex equations, depending on rotor geometries, but the proportionality is always verified between the density of the material and the square of the peripheral speed, $r \cdot \omega$, where r is the radius and $\omega$ the angular velocity.
For this reason flywheel technology hosts two main classes of devices:

- High Speed FESS: in these devices are used light materials to lower density increasing maximum achievable speed (over 100.000 rpm).
- Low speed FESS: robustness in terms of maximum tensile strength is preferred over speed (up to 10.000 rpm).

It is demonstrated that higher energy capacities are reached for devices with low density and high tensile strength (High Speed class). At the same time faster FESSs are characterized by better overall efficiency but require use of advanced technologies that drives up prices (especially in terms of bearings).

Depending on the type of application one type is preferred over the other: for example in transportation applications, the first type is preferred to lower the total mass of the device. The choice of the type of flywheel, and more specifically of the of materials used will be a result of a post-processing

analysis.

For the application of this study it could be preferable to choose choose a low speed flywheel. The preference is guided by the fact that "the price of high speed flywheels can be up to five times higher than the cost of low speed flywheels". [32] [34]

# 4 Models of Degradation

The optimization aims to improve battery life through an effective calculation of the cost of the degradation of the storage devices. The degradation model complexity depends greatly on the type of storage used: while a simple correlation can be used for flywheel, more complex dependencies has to be taken in account for Lithium-Ion technology. In fact, electro-chemical batteries are complex devices, and degradation is dominated by high degree of non-linearity.

## 4.1 Degradation Model for Lithium Ion Battery

Typically the aging process of the battery can be divided into two components: calendrical aging and Operational aging [35]. Calendrical aging is time-dependent and is mainly affected by

- Ambient Temperature;
- Open Circuit Voltage: directly proportional to the State of Charge;

### 4.1.1 Calendrical aging

Generally, storing energy at high SoC and High Temperature reduces battery life-time. While the Ambient Temperature can be controlled by means of AC systems, the effect on degradation by the mean SoC has to be taken in account. From literature review and empirical studies it can be quantified the effect of the average State of Charge on the Irreversible Capacity loss of the battery [36] [37] [38]. For example, the loss in SoH of Lithium-Ion cells results to be considerably more pronounced for SoH higher than 40% [39].
The irreversible loss keeping fixed the temperature at 40°C is greatly affected by the average SoC of the battery: the results observed by [36] from accelerated aging tests, are observable in Figure 3.

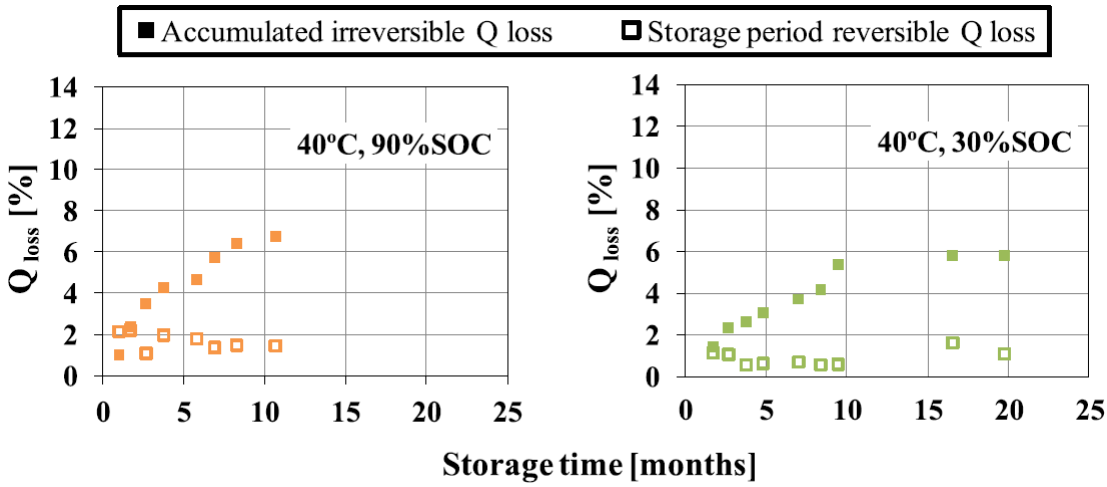


Figure 3: Cumulative Energy Loss [36].

After ca 10 months of storage the unrecoverable loss is 10.5% at 90%, while only 6.4% if kept at 30% of its maximum SoC.

### 4.1.2 Operational aging

Operational aging is the usage-dependent component of degradation, mainly dependent on:

- C Rate;
- Average State of Charge.

It was investigated the degradation based on cycles with a cycle depth of 10% around different average SOC. Results can be observed in Figure 4.

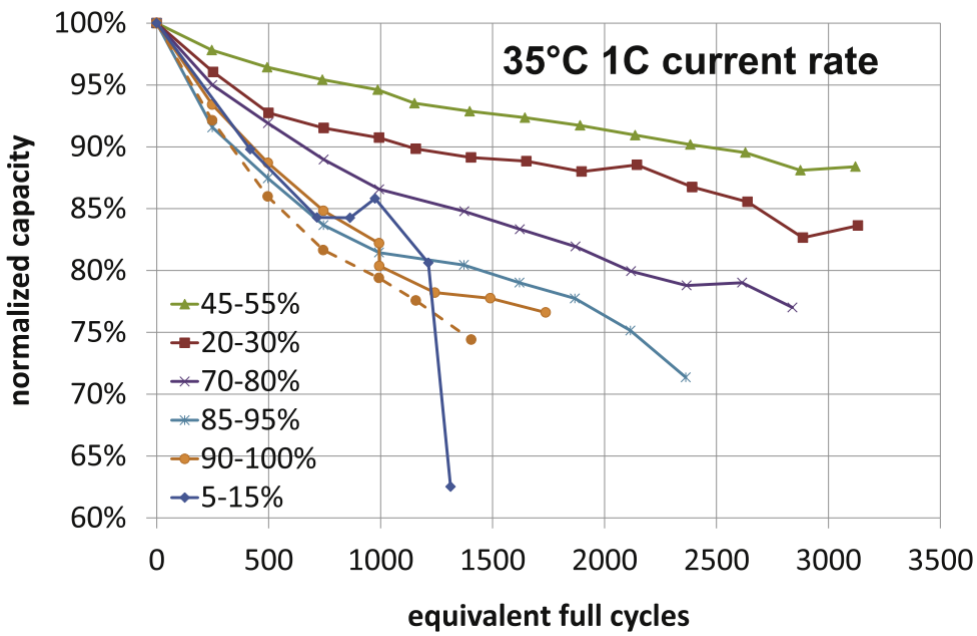


Figure 4: Normalized capacity vs. equivalent full cycles for cells cycled with 1 C at a cell temperature of 35 °C [38].

#### 4.1.3 Battery Degradation Model Applied

In a first stage, to apply a model simulating the degradation of the battery during the optimization phase in GAMS, a simple strategy has to be applied. The preferred choice takes in account the calendrical degradation component, being simple and effective for computational requirements. The first parameter to be calculated is named Average Cost of Degradation $C_{ave}$ [€/kWh], which represents the capital specific cost of the battery [€/kWh] (specific capital predicted cost in 2030 $\lambda_{Bat2030}$) divided by the time steps of the expected lifetime of the device currently used [40]. This cost does not represent correctly the real degradation during one time step, since it does not include any information on the operational conditions at which battery is operated, or in other words, at which SoC(t) the battery is kept for that instant of time. The correlation is developed in two ways: a simple linear model and a quadratic function, resulting from a curve fitting process.

**Linear Model**

The linear model correlation is defined assuming that the $C_{ave}$ is associated with an average State of Charge equal to 50%. This choice was guided by the fact that Lithium Ion batteries experience lower stress from discharge cycles around 50% [36]. At this point is simply assumed that a value of

$SoC = 0\%$ is associated with no degradation of the battery. Finally the Linear degradation cost can be expressed in Equation 2

$$C_{DB} = 2 \cdot C_{ave} \cdot X \tag{2}$$

- X is the average State of Charge, in kWh during the day.

**Quadratic Model**

The quadratic function takes in account the input data provided by the accelerated aging tests in [38]. The specific cost of calendrical degradation applied for the time period of one day, for one kWh of Lithium-Battery is calculated as the following quadratic function:

$$c_{DB} = 0.00976 \cdot x^2 + 0.01896 \cdot x + 0.00223 \tag{3}$$

where:

- $c_{DB}$ is expressed in €/kWh;
- x is the average state of charge in p.u.

This value is finally multiplied by the size of the battery to obtain the real economical loss of degradation:

$$C_{DB} = Cap_B \cdot c_{DB} \tag{4}$$

## 4.2 Degradation Model for Flywheel

For the flywheel a simple model is taken in account, assuming that the energy throughput will be unchanged varying the operational strategy:

$$c_{DF} = \frac{C_{2030}}{E_t} \tag{5}$$

The calculation takes in account the expected specific cost of flywheel technology in 2030 [40], dividing it by the energy throughput $E_T$, calculated as:

$$E_t = N_{cycles} \cdot Cap_F \tag{6}$$

For the purpose of the calculation the term $Cap_F$ indicating the energy capacity of the flywheel is taken to be the unity in kWh. Therefore the cost of degradation is expressible in €/kWh.

# 5 Optimization Model

## 5.1 Overview

The problem to be solved is articulated in two areas of resolution:

- Size of HSS;
- Definition of the operational strategy.

The degree of complexity of the optimization is increased by the fact that both resolutions have to be solved simultaneously. Moreover, given the economical and regulatory framework described in Section 2, the author opted to consider in the investigation the Day-Ahead Market scheduling and the Deviation Imbalance payments. In Figure 5 can be observed the Market phases highlighting the stages taken in account for the purpose of this investigation.

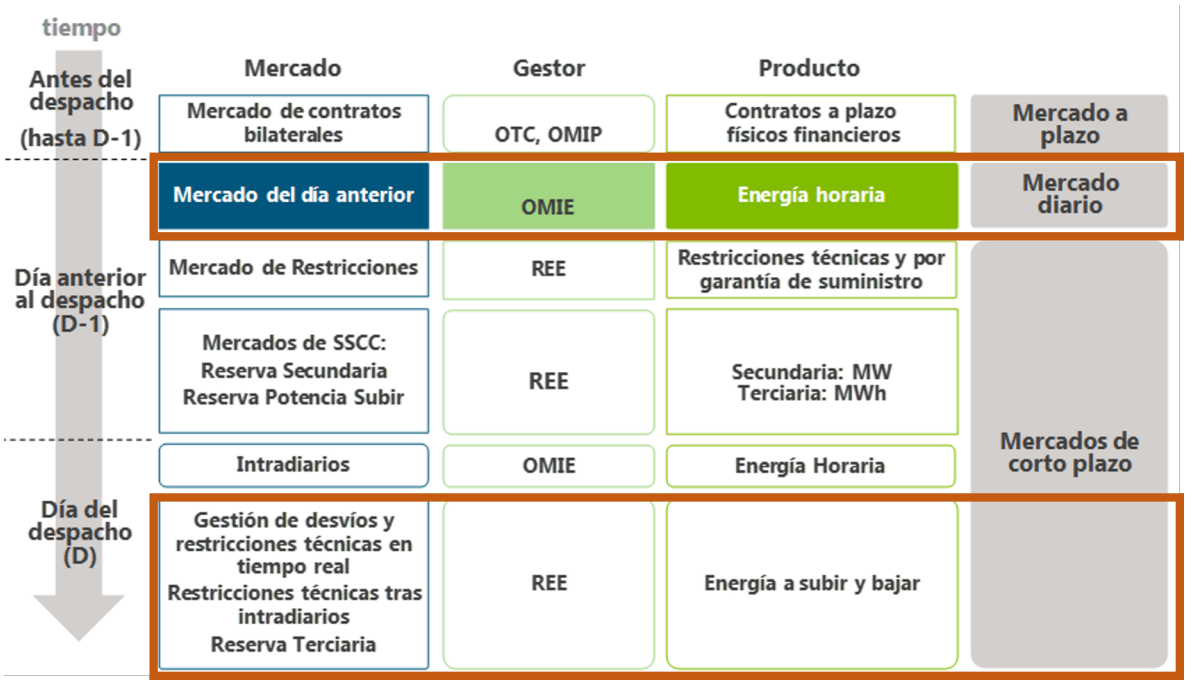


Figure 5: Market strategy adopted.

It is important to highlight that in a real market operation, particular weight is given also to Intra-day market operations, that present scheduling adjustment possibility and a large margin of improvement in terms of profitability for a PVPP operator. Given the choice of the market strategy, the optimization

problem is therefore split into two time-based problems:

- Day-Ahead Schedule;
- Real time Deviation Management.

In other words, these problems are articulated and have to be pragmatically solved through the computation of two optimization steps:

1. Given a weather forecast prediction, is calculated a predicted oower output of the PVPP. Through the first optimization step it is calculated what would be the optimal Day-Ahead Market strategy and the size of the HSS that will allow to maximize the profit.
2. The predicted market strategy is fed in a second optimization, that takes in account the real irradiation data, and calculates, once again, both the operational strategy and the size of the HSS, maximizing the profit but taking into account also the deviation due to forecasting error.

The computation of the HSS size in the second optimization step, is constrained to some degrees around the first solution found. This strategy is chosen on the one hand to better adapt the size of the storage, while on the other hand to not alter substantially the hybrid scheme setup. In Figure 6 the double optimization process described is referred as *Offline* since historical data can be processed and fed into the optimizations to correctly size the HSS.

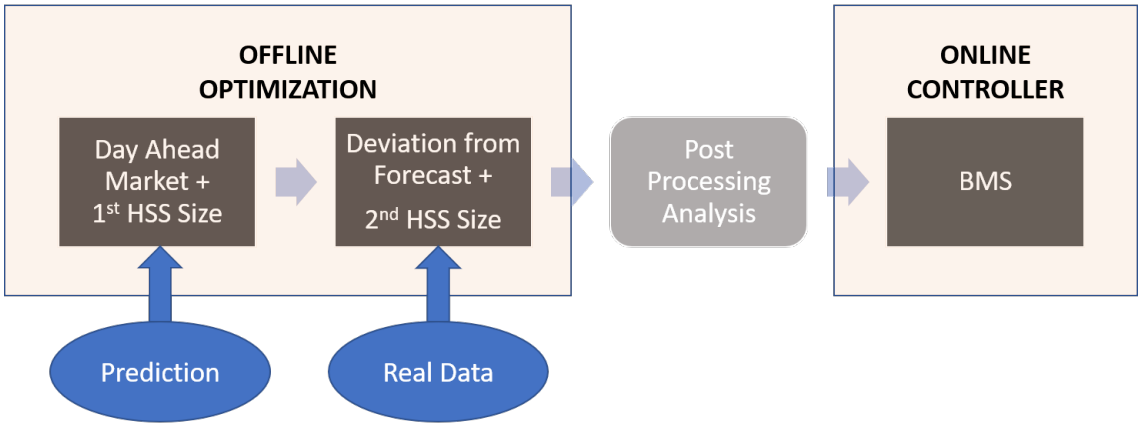


Figure 6: Overview of the Solution Developed

The results obtained are compared with a base case scenario in which no storage system is coupled with the PVPP.

## 5.2 Assumptions

As already discussed in Section 2.3.1, the minimum power to be bid in the FCR market is 1 MW. Bids are performed monthly, therefore there is possibility for the plant operator to adjust the bidding power reserve $P_{bid}$ and the time range $h_{bid}$ to the optimal solutions provided by the optimization.

On this regard, it has to be taken in account that the solution is referred to one day only: irradiance data can vary largely throughout the year, leading to different optimal values of $P_{bid}$ and $h_{bid}$. Moreover, due to the optimization problem definition, it was necessary to define these two values, before the resolution as starting points. A meaningful choice should take in account the following considerations:

1. Once set, both $P_{bid}$ and $h_{bid}$ will deeply affect the size and the operational strategy of the solution.

2. As a matter of fact and consequently: a lower choice of $P_{bid}$ leads to lower storage capacities.

Logically, both lower $P_{bid}$ and $h_{bid}$ lead to lower energy input to the HSS to be able to supply enough reserve in the bidding time - period.

While the operational strategy can be changed day by day depending mainly on the solar resource prediction and the market conditions, the size is a fundamental limit for the the capability of the system to provide FCR service, and therefore to the profitability of the plant.

On the other hand, it is important to emphasize that FCR is intended a secondary service to be coupled with normal PVPP operations: from simulations results it is observed that most of the yearly earnings comes from the energy sold in the daily ahead market (not from ancillary services, as it could be expected). Therefore, both from a technical and an economical perspective,the assumption of $P_{bid}$ and $h_{bid}$ should have a double aim:

- Decrease as much as possible the initial investment cost;
- Maximize the yearly period of time in which the FCR service can be performed profitably.

These two aims are directly connected: in fact the choice to minimize the investment cost, therefore the size of the HSS, ultimately reduces also the risk to oversize the reserve for periods of the year with less solar resource (less solar radiation, less PFC power requirements etc.). Moreover, it is clear that, once the system is sized, the capability to provide FCR service depends only on the operational strategy adopted.

As a consequence of the analysis presented above, and after analysing the solar resource data for the month of April (use case) it is assumed that:

- the Power Reserve $P_{bid}$ is constrained to the minimum viable value of 1 MW.
- the amount of hours to be bid $h_{bid}$ during the day is chosen to be $4\ hours$.

The strategy is graphically showed in Figure 7.

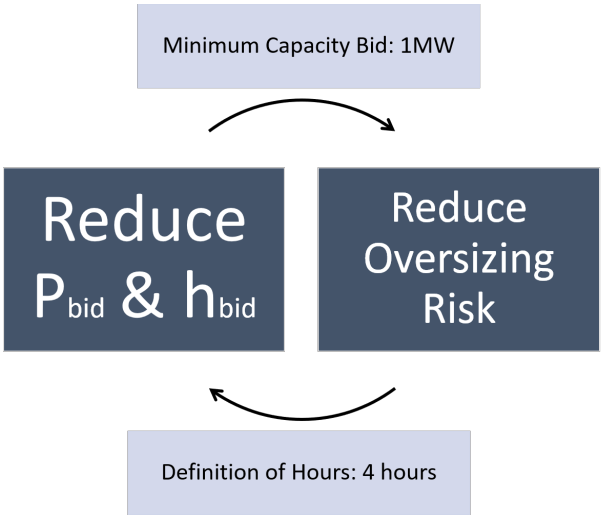


Figure 7: Overview of the chosen sizing strategy.

A sensitivity analysis on this regarding is the object of Section 6.5.

## 5.3 Input Data

### 5.3.1 Irradiation and Power output

The power plant investigated is 9.4 MW, a real case of PVPP in Romania [41]. The input data for the irradiation is extrapolated for simplicity from NREL database, taking in account the Global Horizontal Irradiation data from the OAHU Solar Measurement station [42]. The data-set has a second-by-second resolution: for the intended outcomes of the investigation, the data is filtered every 15 seconds, reducing data to 5760 irradiation values. At this stage it is necessary to create a simple model to evaluate the power output, given the irradiation as input. It is known by literature that PV power output fluctuations reduce as the plant size increases [43]. Therefore the irradiation is fed in a low-pass filter model to obtain directly an estimated power output. The transfer function is shown in Figure 8.

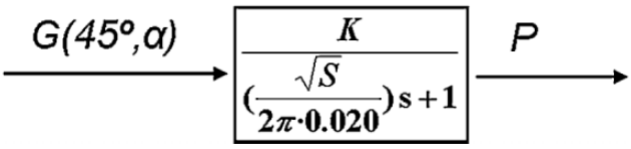


Figure 8: Proposed transfer function for a PV plant with an area equal to S [43].

The area estimated for this power plant is $S = 52$Ha. The gain K is used in order to scale the power output and is equal to the nominal power rating of the plant $K = 9.4$ MW.

The output can be observed in Figure 9.

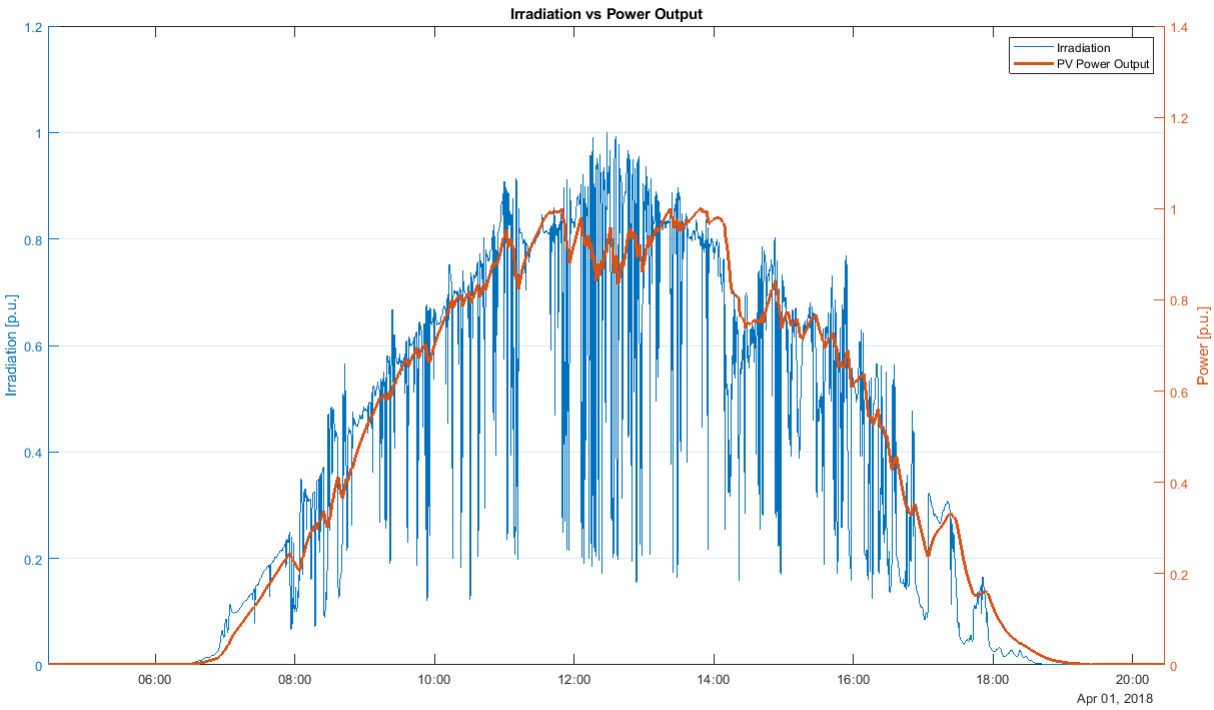


Figure 9: Input data: Irradiation and PV Power Plant output.

### 5.3.2 Day-Ahead Prediction

The prediction of the power output to schedule the bidding in the day ahead market is not a trivial problem.

"High-quality weather forecasting can accurately predict output on a two- to six-hour interval, greatly improving system reliability. Today, forecast errors typically range from 3% to 6% of the rated capacity an hour ahead and from 6% to 8% a day ahead on a regional basis (as opposed to for a single plant)." [4]

It is clear that even a slight increase in forecasting accuracy has great potential to result in large economic benefits. "By using the significant processing power afforded by modern ICT, such as cloud-based computing, improved mathematical models (which produce forecast results for 5 or 15 minutes instead of an hour) and artificial intelligence, together with the big data collected on past weather pat-

terns and generation outputs, accuracy and locational resolution of VRE generation forecast could be improved." [4]

Indeed, for the scope of this project a simple forecasting method is chosen: it is possible to calculate the rRMSE (relative Root Mean Square Error) of the power output of the plant given the irradiance: the relationship showed in Figure 10 shows a direct proportion between the error and the magnitude of the sun irradiance.

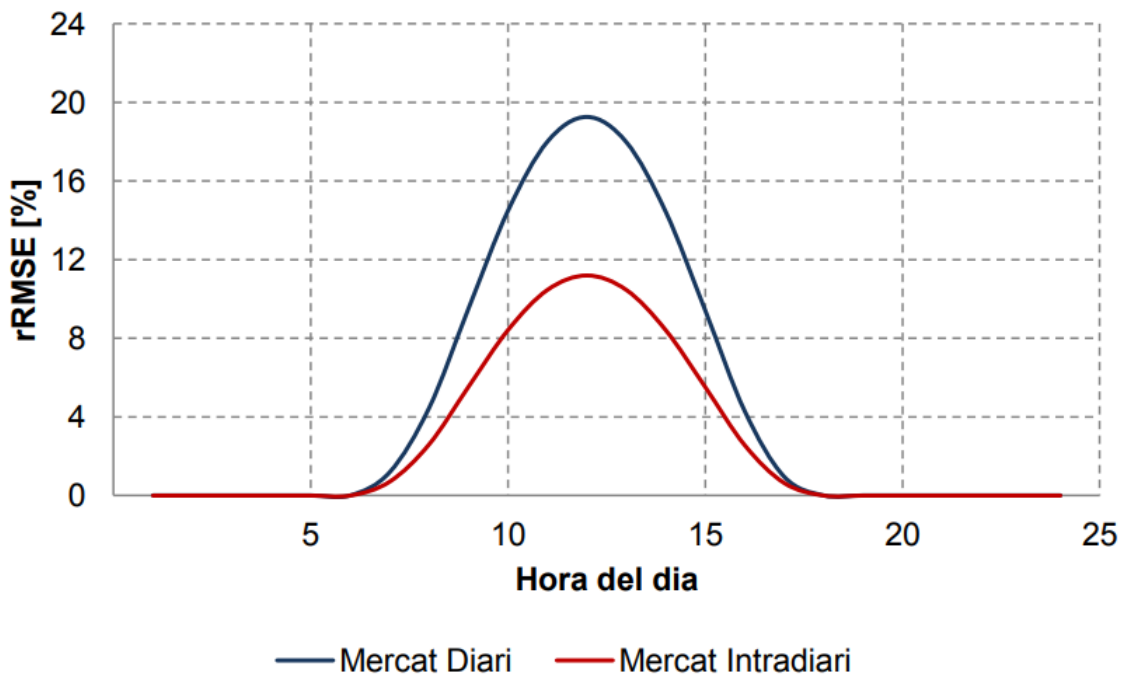


Figure 10: Firm Frequency Response overview [44]

Therefore the input for the prediction is the average hourly irradiation: this is used to calculate for every hour the rRMSE. The hypothesis takes in account that the weather forecast can accurately predict hourly irradiation in the short term (day-ahead), but it is impossible to predict the irradiation with the time step used in the simulation (15 s). To calculate the rRMSE the average hourly irradiation is normalized with the maximum irradiation value of the day and is multiplied by 19% [44]. The error is then used to calculate the predicted hourly energy produced: through a random binary variable, each hour the error is applied summing or subtracting the error made in the prediction. Equation [**?**] synthesizes the approach followed.

$$E_{pred}(h) = E_{max} \cdot I_{real}(h) \cdot (1 + rRMSE(h) \cdot B(h)) \tag{7}$$

where:

- $E_{pred}$ is the hourly predicted energy output;
- $E_{max}$ is the maximum energy registered in a time step;
- $I_{real}(h)$ is the average hourly irradiation;
- $rRMSE(h)$ is the relative Root Mean Squared Error;
- $B(h)$ is a random integer variable that can assume values (-1;+1).

Finally, every 15 seconds a noise is added to render the data more realistic. The noise is calculated through a normal distribution, using as a standard deviation the hourly standard deviation of the real energy produced. The final result has been adapted with a low-pass filter (time constant=30 s) in order to take in account the softening effect of the large size of the PVPP. The energy trend can be observed in Figure 11.

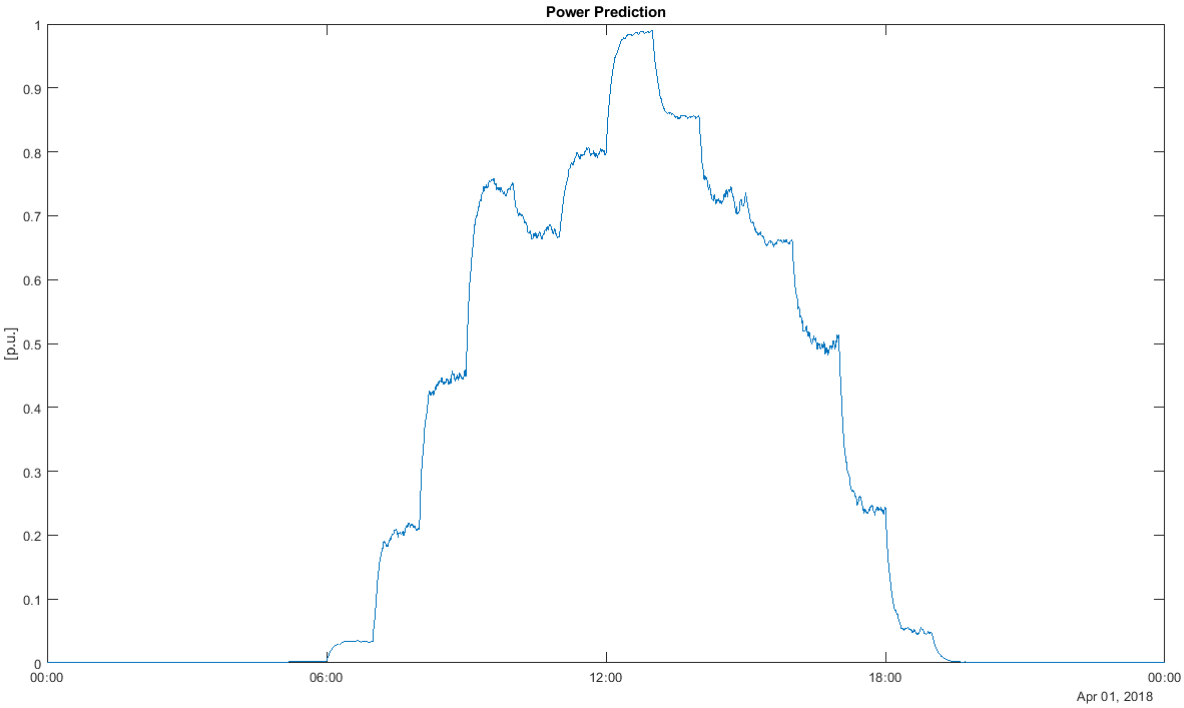


Figure 11: Predicted energy day ahead

### 5.3.3 Frequency

The ancillary service provided by the Energy System (PVPP + HSS) studied in this thesis is primary frequency control, following UK market guidelines as in detail explained in Section 2.3.1. The frequency input data is supplied by UK TSO, that offer frequency values with 1-second resolution [24]. For the purpose of this research, and to decrease the computational power needed to solve the optimization the values is extrapolated each 15 seconds. The input data is shown in Figure 12.

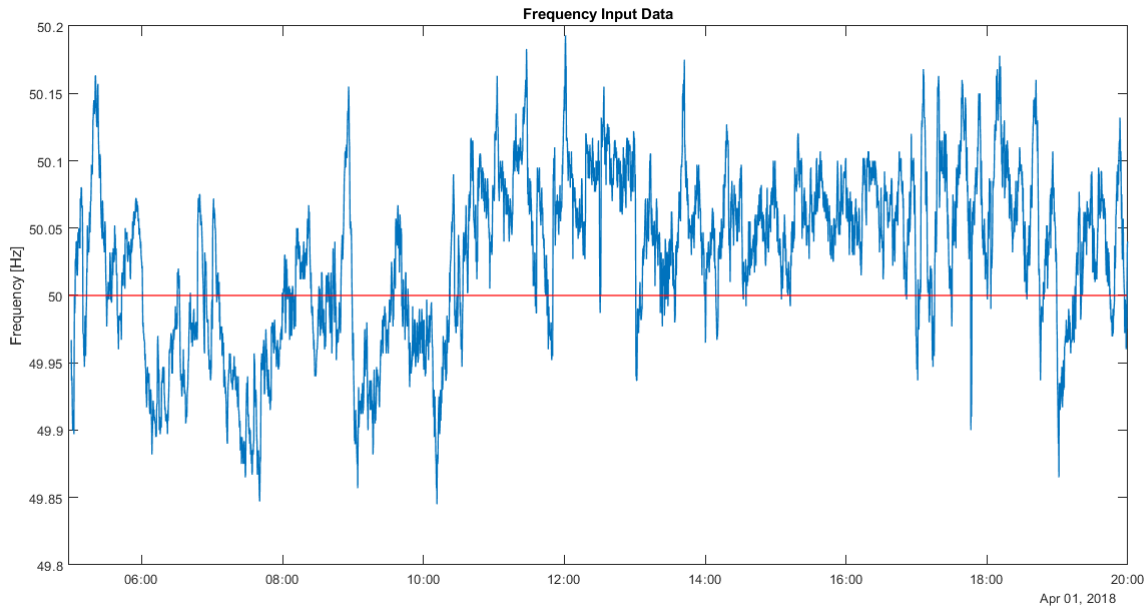


Figure 12: Frequency on 01.04.2019 in UK grid.

Referring to Section 2, it is chosen a market mechanism that compensate the FCR as the UK Firm Frequency Response but respect the indication of the ENTSO-E and the Spanish Regulatory Framework in terms of time-response and frequency control droop.

**Assumptions**

Given these choices there is still one degree of freedom in market regulations: the frequency control droop does not state clearly the value of the reserve magnitude, that is explained in Section 2.2.1 to be allowed between 1.5% to 10%. The worst case scenario is chosen: in each time step the PVPP has to provide **PR** with 10% of the available power output continuously and free of economical compensation.

**Calculation of the frequency response**

At this stage the frequency trend during the day under analysis, together with the PV power output of the PV plant, is used to quantify the power requested to ensure the Primary Frequency Control. The plant has to provide part of the actual power output for frequency deviation, following indications in Table 2. But when the plant is actively participating in the FFR service (UK regulation), the power to be provided is not anymore dependent on the power produced, but proportional to the Power reserve bid in the Ancillary Market. The final result of power needed for frequency control is shown in Figure 13.

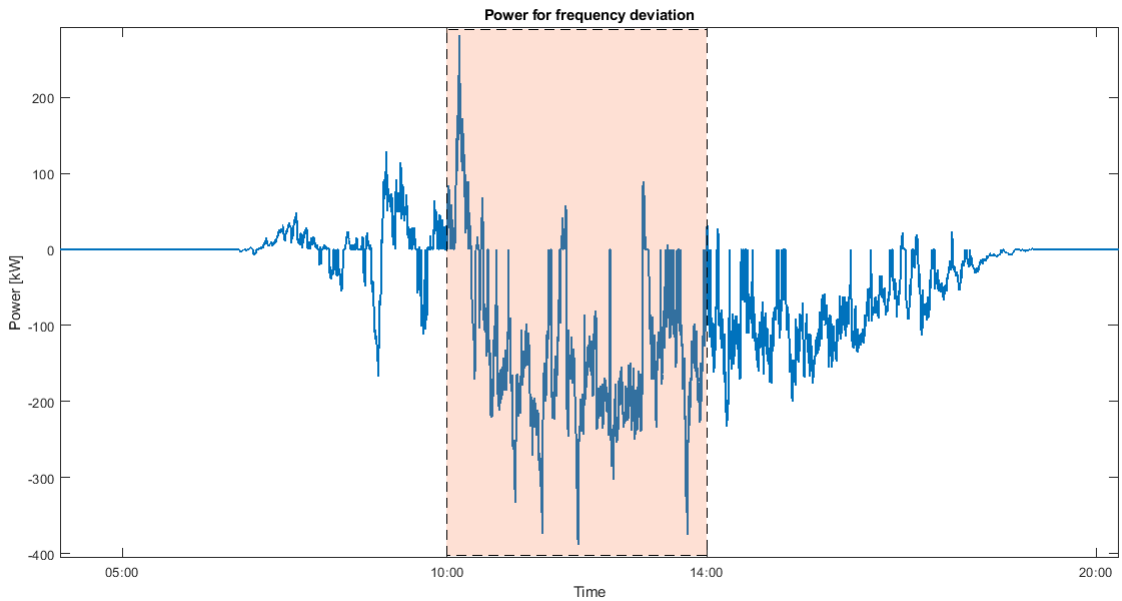


Figure 13: Power response for PFC every 15 s. It is highlighted the time range in which the power response is not dependant on the PV production or bidding time.

It is possible to observe that this day is characterized by an overfrequency behaviour.

### 5.3.4 Market and Prices

The prices taken in account for the purpose of this study refer to the Spanish Market. Data are downloaded from the ESIOS website [45], in particular the following data are necessary to economically quantify the revenue stream from the service provided by the PVPP Operations:

- Daily-Ahead Market price: defined hourly in the Daily Ahead auction Market. Indicated as

$\lambda_M$(h) [€/MWh];

- System necessity, defined hourly. For the purpose of the optimization is defined as a binary variable $N$(h). When the system is experiencing an overproduction, or in other words, the demand is lower than the generation, $N = 1$;

- Deviation price (in case of overproduction) and deviation cost (in case of lower production).

It is important to highlight that the price variability throughout the day investigated is small compared to other days of the month, as it is possible to observe from Figure 14

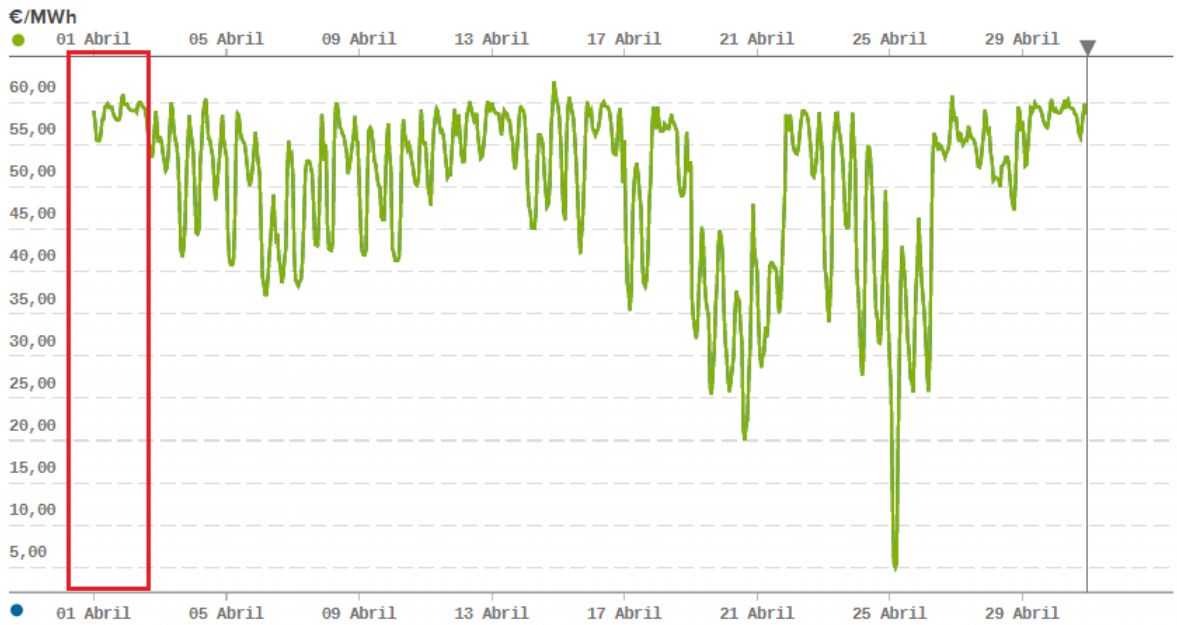


Figure 14: Price trend during April 2019 [45].

From this evaluation can be concluded that arbitrage will not be preferred as a main strategy for the HSS, since shifting energy from one hour to another could be not a remunerative choice for the optimization program.

## 5.4 Model Definition

The optimization models built in GAMS are here presented. As already discussed, each scenario presents two phases: prediction and real time optimization. For this reason, the equations in the next

sections are presented (where necessary) in two versions:

- a. Prediction: in which are used the results from Section 5.3.2;
- b. Real time: making use of the real input data.

The objective function is the Profit $P$: revenues $R$ of the plant minus the total costs $C$ over the time period considered.

$$P = R - C; \tag{8}$$

The function profit $P$ has been optimized on an annual basis in order to take in account the different expected technological lifetimes of the flywheel and the battery.

### 5.4.1 Base Case Scenario

The first scenario modeled assume no HSS coupled with the PVPP: as explained in Section 5.1, the base case serves as an economical instrument to measure the effectiveness of the solution adopted.

**Objective Function**

Since no FCR service is provided, as described for UK regulations, the only source of income for the plant comes from the energy sold in the day-ahead market. Daily revenues are calculated in the following ways:

- a.

$$R = R_M = \sum_{t=1}^{5760} \lambda_M(t) \cdot E_M(t); \tag{9}$$

- b.

$$R = R_M = \sum_{t=1}^{5760} \lambda_M(t) \cdot E_M(t) - \sum_{h=1}^{24} D(h); \tag{10}$$

  where:

  - $\lambda_M(t)$ is the market price at time t in €/MWh;
  - $E_M(t)$ is the energy sold to the wholesale market in MWh, defined in Equation 11.
  - $D(h)$ is the hourly deviation from the Day-ahead Market, result of the Base Case Optimiza-

tion **a**. The calculation of the term is shown in Equation 11

$$D(h) = \Big[E_M(h) - E_{Mpred}(h)\Big] \cdot \Big\{ \Big[G(h) \cdot N(h) \cdot \lambda_{up}(h)\Big] + \Big[\Big(1 - G(h)\Big) \cdot N(h) \cdot \lambda_M(h)\Big] + \Big[G(h) \cdot \Big(1 - N(h)\Big) \cdot \lambda_M(h)\Big] + \Big[\Big(1 - G(h)\Big) \cdot \Big(1 - N(h)\Big) \cdot \lambda_{down}(h)\Big] \Big\}$$

where:

- $E_M(h)$ is the hourly energy to be sold during the day of the study in MWh;
- $E_{Mpred}(h)$ is the hourly energy predicted to be sold in the DAM in MWh;
- $G(h)$ is a binary variable calculated comparing the actual hourly generation with the predicted energy to be sold on the DAM: it is equal to 1 when the generation is greater than the prediction $\Big(E_M(h) > E_M(h)_{pred}\Big)$;
- $N(h)$ is a binary variable that gives information regarding the system necessity: is equal to 1 when there is an excess of generation in the electrical system;
- $\lambda_{up}$ is the upward imbalance price in in €/MWh, corresponding to condition 4 in Figure 1;
- $\lambda_{down}$ is the downward imbalance price in €/MWh, corresponding to condition 2 in Figure 1;

Since all scenario evaluated in this thesis take in account the same PVPP size with the same operational costs, in the base case scenario no costs are subtracted to Revenues $R$, therefore is set $C = 0$.

**Global Balances**

1. Market Energy:

$$E_M(t) = PV_{OUTmax}(t) - PV_{RES}(t) - PV_{OFR}(t) \tag{11}$$

where:

- $PV_{OUTmax}$ is the maximum energy output from PV plant in each time step t in MWh;
- $PV_{RES}(t)$ is the upward reserve in MWh, by regulation calculated as:

$$PV_{RES}(t) \geq 0.1 \cdot PV_{OUTmax} \tag{12}$$

$$PV_{RES}(t) \leq 0.15 \cdot PV_{OUTmax} \tag{13}$$

- $PV_{OFR}$ is the energy in MWh for primary frequency control due to upward frequency deviation. The frequency increase forces the inverter to decrease the energy production sold in the Energy Market.

2. Ramp Rate: the value of the ramp rate is 10% of the nominal power each minute, in accord with real applications in several countries [41]. Traditionally, moving average method is used to gradually change of output active power in PV inverter [7], but this strategy is been proved difficult to apply in GAMS environment. Therefore a more restrictive constraint is evaluated: in each time instant the ramp rate constraint is applied equally and proportionally to the duration of the time-step itself (compared to the minute-constraint). The Equations 14 and 15 shows the expression.

$$E_M(t+1) - E_M(t) = 0.025 \cdot \frac{P_{PV}}{s} \tag{14}$$

$$E_M(t) - E_M(t+1) = 0.025 \cdot \frac{P_{PV}}{s} \tag{15}$$

where:

- $P_{PV}$ is the nominal Power of the PVPP in MW;
- s is the number of time-steps in one hour.

### 5.4.2 Linear Degradation Scenario

The Linear model is only applied since the optimization process for the Quadratic Degradation scenario appeared to be slow, particularly in the real time phase.

**Objective Function**

Daily revenues are calculated adding to the market revenues, the frequency compensation for the primary frequency service:

$$R = R_M + R_F \tag{16}$$

where:

- $R_M$ is the market revenue, calculated as:
- a.

$$R_M = \sum_{t=1}^{5760} \lambda_M(t) \cdot E_M(t); \tag{17}$$

- b.

$$R_M = \sum_{t=1}^{5760} \lambda_M(t) \cdot E_M(t) - \sum_{h=1}^{24} D(h); \tag{18}$$

where:

$E_M(t)$ is the energy sold in the Day-Ahead Market calculated as in Equation 25

- $R_F$ is the frequency revenue, calculated as follows:

$$R_F = \lambda_{UFR}(t) \cdot E_{UFR}(t) + \lambda_{av} \cdot P_{bid} \cdot h_{bid} \tag{19}$$

where:

  - $\lambda_{UFR}(t)$ is the frequency response price at time t in €/MWh for under-frequency events;
  - $E_{UFR}(t)$ is the energy required for frequency control during the bidding period in case of downard deviation in MWh;
  - $\lambda_{av}$ is the availability fee in €/$MW\cdot$ h for providing $1MW$ of power capacity for primary frequency control for 1 hour, defined as in Section 5.3.4;
  - $P_{bid}$ is the power reserve in MW that the Power Plant is able to supply for the bidding period.
  - $h_{bid}$ is the time period daily bid in for FCR services, in hours.

The yearly Cost function $C$ is described by following terms:

$$C = C_C + C_D \tag{20}$$

where:

- $C_C$ is the capital investment cost of the HSS:

$$C_C = C_E + C_P \tag{21}$$

where:

- $C_E$ is the capital investment cost of the HSS in terms of energy excluding power electronics (divided into battery and flywheel respective costs):

$$C_E = Cap_{Bat} \cdot \lambda_{Bat} + Cap_{Fly} \cdot \lambda_{Fly} \tag{22}$$

  where:

  * $Cap_{Bat}$ and $Cap_{Fly}$ are respectively the Battery and Flywheel Energy Capacity in terms of kWh;
  * $\lambda_{Bat}$ and $\lambda_{Fly}$ are respectively the Battery and Flywheel specific costs of the energy storage devices.

- $C_P$ is the cost in terms of power capacity and includes the price of power electronics:

$$C_P = P_{HSS} \cdot \lambda_P \tag{23}$$

  where:

  * $P_{HSS}$ is the overall storage Power capacity in terms of kW;
  * $\lambda_P$ is the specific cost of the power electronics devices.

- $C_{DB}$ is the degradation cost, that accounts for the use of the battery and its consequent degradation. This cost has been discussed in Section 4, and it has to be intended as a virtual cost: since the degradation does not produce any real neither present cost, but can influence the time in which the battery has to be substituted, this cost has been obtained by the expected cost of the battery in 2030. As already discussed, the cost of degradation of the battery $C_{DB}$ depends on the mean state of Charge, and it is calculated as in Equation 2. Flywheel degradation cost $C_{DF}$ is proportional to the energy output of the flywheel:

$$C_{DF} = \sum_{t=1}^{5760} c_{DF} \cdot F_{Ufr}(t) \tag{24}$$

  where $c_{DF}$ has been calculated in Equation 5 while $F_{Ufr}$ is the energy output of the flywheel, described in Equation 29.

**Global Balances**

1. Market Energy:

$$E_M(t) = PV_{out}(t) + B_M(t) \cdot \varepsilon_{Bout} - B_{PV}(t)/\varepsilon_{Bin} - F_{PV}(t)/\varepsilon_{Fin} \tag{25}$$

where:

- $PV_{OUT}$ is the net energy released from the PV in MWh calculated in Equation 30;
- $B_M(t)$ is the energy in MWh discharged from the battery for deviation imbalance minimization and arbitrage service; calculated as in Equation 37;
- $\varepsilon_{Bout}$ accounts for losses of discharge of the battery;
- $B_{PV}(t)$ is the share of energy input to the battery directly injected from the PV, and adding up to the $SOC$ in MWh;
- $\varepsilon_{Bin}$ accounts for losses of charge of the battery;
- $F_{PV}(t)$ is the share of energy input to the flywheel directly injected from the PV, and adding up to the $SOC$ in MWh;
- $\varepsilon_{Fin}$ accounts for losses of charge of the flywheel.

After successive GAMS iterations it was decided to add on top of the PFC, the capability of arbitrage for the Battery, represented by the $E : M$ in order to freely optimize the energy use throughout the day, reducing forecast errors and shifting the Energy sold in DAM when more convenient. The arbitrage function of the battery is investigated furthermore in Section 6.2.

2. Ramp Rate: the Equations 14 and 15 defined for the Base Case are valid for this model too;

3. Reserve for ENTSO-E Regulation:

$$PV_{res}(t) + B_{us}(t) \cdot \varepsilon_{Bout} + F_{us}(t) \cdot \varepsilon_{Fout} \geq 0.1 \cdot PV_{outmax}(t) \tag{26}$$

This constraint ensure that in any moment there is sufficient energy to cover a large frequency drop. Differently from the Base Case Scenario this energy can be supplied from the HSS.

- $B_{us}(t)$ and $F_{us}(t)$ are the operable energy in each time step t in MWh, defined in Equations 43 and 52;
- $\varepsilon_{Fout}$ accounts for losses of discharge of the flywheel;

4. Reserve for FCR Primary and Secondary Service:

$$B_{us}(t) \cdot \varepsilon_{Bout} + F_{us}(t) \cdot \varepsilon_{Fout} \geq \frac{P_{bid}}{s} \tag{27}$$

In this case the energy to be ensured is contained in the reserves without making use of the solar reserve: this is taken as a safety measure in order to ensure the capability to respond to the worst frequency drop in any moment, independently from the instantaneous PV power output.

5. Under-frequency energy out from bidding range of time:

$$F_{Ufr}(t) \cdot \varepsilon_{Fout} = PV_{Ufr}(t) \tag{28}$$

$\forall t \in \{1\ ,\ bid_{start}\} \wedge \{bid_{end}\ ,\ t_{end}\}$,

- $F_{Ufr}(t)$ is the energy provided by the flywheel for under-frequency events;
- $PV_{Ufr}(t)$ is the energy requested for downard frequency deviation, depending on the available power $PV_{OUTmax}(t)$ and calculated following indications in Table table:frequencyspain
- $bid_{start}$ is the instant of time in which start the bidding period: in the case study is $10AM$;
- $bid_{start}$ is the instant of time in which start the bidding period: in the case study is $2PM$.
- $t_{end}$ is the instant of time corresponding to the end of the simulation ($t = 5760$).

Only the flywheel is responsible for under-frequency events in this time range, while the battery and the PV reserve will complement during large frequency deviations. This mechanism is further explained in Section 7, where the BMS is defined.

6. Under-frequency energy in bidding range of time:

$$PV_{Ufr}(t) + B_{Ufr}(t) \cdot \varepsilon_{Bout} + F_{Ufr}(t) \cdot \varepsilon_{Fout} = Bid_{Ufr}(t) \tag{29}$$

$\forall t \in \{bid_{start}\ ,\ bid_{end}\}$, where: where:

- $PV_{Ufr}(t)$ is the share of PV reserve in MWh used for downward frequency deviations, defined in Equation 33;
- $B_{Ufr}(t)$ is the energy output in MWh from the battery for downward frequency deviations;
- $Bid_{Ufr}(t)$ is the energy requested for downward frequency deviation, independent from the available power $PV_{OUTmax}(t)$ but proportional to the power reserve bid $P_{bid}$.

In this case the frequency variation leads to higher values of energy requested for FCR, therefore it chosen to use the overall HSS including the reserve of the PV panels.

**PV Balances**

Net Energy from PV:

$$PV_{out}(t) = PV_{outmax}(t) - PV_{res1}(t) \tag{30}$$

where:

- $PV_{res1}(t)$ is the reserve that the PV has to provide to provide constantly taking in account also over-frequency events as follows:

$$PV_{res1}(t) = PV_{res}(t) + E_{Ofr}(t) \tag{31}$$

$$PV_{Ofr}(t) = E_{Ofr}(t) - F_{Ofr}(t)/\varepsilon_{Fin} \tag{32}$$

  where

  - $E_{Ofr}(t)$ is the energy requested for over-frequency events;
  - $F_{Ofr}(t)$ is the share of energy that charge the flywheel during over-frequency events: instead of being curtailed, this energy can be temporarily stored in the flywheel.

- Under-frequency definition:

$$PV_{Ufr}(t) \leq PV_{res}(t) \tag{33}$$

  Meaning that the energy for downward frequency deviation cannot overcome the reserve stored through PV output curtailment.

  The reserve is constrained as it follows:

$$PV_{res}(t) \leq 0.15 \cdot PV_{outmax} \tag{34}$$

**Battery Balances**

1. State of Charge Definition:

$$SOC_B(t) - SOC_B(t-1) = B_{in}(t) - B_{out}(t) - B_{loss}(t) \tag{35}$$

   where:

- $SOC_B(t)$ is the State of Charge of the battery at time t, expressed in MWh;
- $B_{loss}$ is the loss due to battery discharge in MWh defined as follows:

$$B_{loss}(t) = \gamma_B \cdot SOC_B(t) \tag{36}$$

  where $\gamma_B$ is the share of $SoC$ that is lost due to self-discharge during a time step of 15s [40].

- $B_{out}$ is the energy discharged from the battery in MWh, defined as follows:

$$B_{out} = B_M + B_{Ufr} \tag{37}$$

In this optimization phase it is not known the battery capacity, therefore the $SOC_B$ is expressed in kWh.

2. Limit of the state of Charge:

$$SOC_B(t) \leq \alpha_{B+} \cdot Cap_B \tag{38}$$

$$SOC_B(t) \leq \alpha_{B-} \cdot Cap_B \tag{39}$$

where:

- $alpha_{B+}$ is the highest State of Charge allowed.
- $alpha_{B-}$ is the lowest State of Charge allowed [46].

3. State of Charge Constraint:

$$SOC_B(1) = SOC_B(t_{end}) \tag{40}$$

The battery is forced to be at the same state of charge at the end of the optimization, in order to perform effectively another day of operations.

4. Average State of Charge:

$$\overline{SOC_B} = \sum_{t=1}^{5760} SOC_B(t) \tag{41}$$

where $\overline{SOC_B}$ is an absolute quantity in MWh;

5. Arbitrage time-constraint:

$$B_M(t) = 0 \tag{42}$$

$\forall t \in \{1\ ,\ prod_{start}\} \wedge \{prod_{end}\ ,\ t_{end}\}$, where:

- $prod_{start}$ is the instant of time corresponding to the beginning of the first hour in which it is registered solar production. In this case 7:00:00 AM;
- $prod_{end}$ is the instant of time corresponding to the end of the hour in which it is registered solar production. In this case 8:59:45 PM

This constraint limit the possibility of arbitrage of the battery inside the time range in which PVPP is actively bidding for the DAM. If the constraint is not applied it is observed a discharging behaviour in the beginning of the day that increase by a small amount the objective function, but is not realistic for the use case.

6. Battery Usable Energy:

$$B_{us}(t) \leq \frac{SOC_B(t)}{\frac{s}{4}} \tag{43}$$

$\forall t \in \{1\ ,\ prod_{start}\} \wedge \{prod_{end}\ ,\ t_{end}\}$, since the Spanish regulation set the event detection time to 15 minutes as described in Section 2.2.1.

$$B_{us}(t) \leq \frac{SOC_B(t)}{\frac{s}{2}} \tag{44}$$

$\forall t \in \{bid_{start}\ ,\ bid_{end}\}$, since the UK National regulator set the event detection time up to 30 minutes for Primary and Secondary FCR as already explained in Section 2.3.1.

7. Simultaneous charge and discharge:

$$B_{in} \cdot B_{out} = 0; \tag{45}$$

This constraint does not allow the system to charge and discharge at the same time the battery.

**Flywheel Balances**

1. State of Charge Definition:

$$SOC_F(t) - SOC_F(t-1) = F_{in} - F_{Ufr} - F_{loss} \tag{46}$$

where:

- $SOC_F(t)$ is the State of Charge of the flywheel at time t, expressed in MWh;
- $F_{in}$ overall energy input to the flywheel adding up to the SoC in MWh, and defined as follows:

$$F_{in}(t) = F_{PV}(t) + F_{Ofr}(t) \tag{47}$$

- $B_{loss}$ is the loss due to battery discharge in MWh defined as follows:

$$F_{loss}(t) = \gamma_F \cdot SOC_F(t) \tag{48}$$

where $\gamma_F$ is the share of $SoC$ that is lost due to self-discharge during a time step of 15s [40].

The state of charge definition is similar to the one modelled for the battery in Equation 35 but the definition of each variable is different. In fact, given the different characteristics of the flywheel, such as high power capabilities and fast responsive behaviour, the device is set to be in charge of frequency deviations. Without the flywheel this energy would be simply curtailed by the MPPT control of the PV, as shown in Equation 31.

2. Limit of the state of Charge:

$$SOC_F(t) \leq \alpha_{F+} \cdot Cap_F \tag{49}$$

$$SOC_F(t) \leq \alpha_{F-} \cdot Cap_F \tag{50}$$

where:

- $\alpha_{F+}$ is the highest State of Charge allowed.
- $\alpha_{F-}$ is the lowest State of Charge allowed.

3. State of Charge Constraint:

$$SOC_F(1) = SOC_F(t_{end}) \tag{51}$$

Also the Flywheel is constrained in this way to maintain its state of charge at the beginning and at the end of the day.

4. Battery Usable Energy:

$$B_{us}(t) \leq \frac{SOC_B(t)}{\frac{s}{4}} \tag{52}$$

$\forall t \in \{1\ ,\ prod_{start}\} \wedge \{prod_{end}\ ,\ t_{end}\}$

$$B_{us}(t) \leq \frac{SOC_B(t)}{\frac{s}{2}} \tag{53}$$

$\forall t \in \{bid_{start}\ ,\ bid_{end}\}$

5. Simultaneous charge and discharge:

$$F_{in} \cdot F_{Ufr} = 0; \tag{54}$$

### 5.5 Parameters

The techno-economic parameters chosen from literature review are shown in this section and summarized in Table 3.

| Parameters | | |
|---|---|---|
| Quantity | Value | Unit |
| s | 240 | |
| $\lambda_{Bat}$ | 420 | €/kWh |
| $\lambda_{Bat2030}$ | 150 | €/kWh |
| $\lambda_{Fly}$ | 3000 | €/kWh |
| $\lambda_{Fly2030}$ | 1959 | €/kWh |
| $\lambda_P$ | 160 | €/kW |
| $\varepsilon_{Bin} = \varepsilon_{Bout}$ | 0.975 | |
| $\varepsilon_{Fin} = \varepsilon_{Fout}$ | 0.917 | |
| $\alpha_{B+}$ | 1 | |
| $\alpha_{B-}$ | 0.1 | |
| $\alpha_{F+}$ | 1 | |
| $\alpha_{F-}$ | 0.15 | |

Table 3: Chosen Parameters for GAMS model

# 6 Optimization Results

In this section are shown the results from the GAMS optimizations and it is evaluated the strategy to build up the control system for the battery and the flywheel.

## 6.1 Base Case

The base case scenario present low or no degree of freedom in terms of operational strategy.

1. The prediction step aims simply to maximize the energy sold in the market, given the constraints in Equations 11 and 12

2. The real time phase strategy aims to maximize $E_M$ while minimizing the error from forecast, given the possibility to adjust the MPPT of the solar converter as in Equations 12 and 34

**Prediction**

Figure 15 shows the maximum solar resource for the case of prediction, the reverse to comply with Spanish operator and the actual Energy sold on the market.

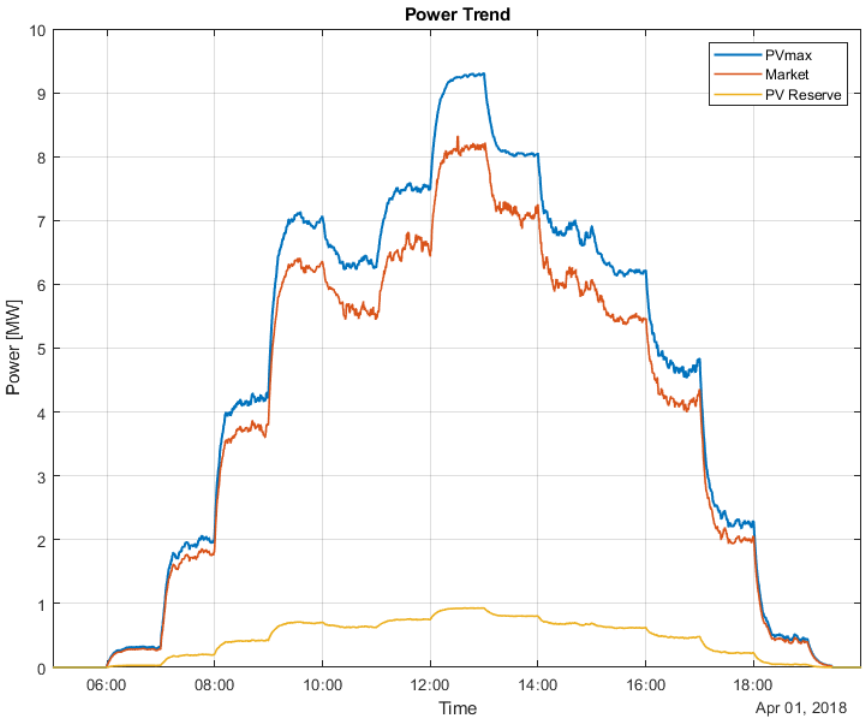


Figure 15: Prediction step: Power trend over the day.

It is observable that the reserve level of the PV through the MPPT is quite consistent and represents an economical loss for the plant operator. One question that could be raised at this point is: how much of this reserve for frequency deviation is actually being used? To answer to this question it was compared in Figure 16 the normalized reserve level with the under-frequency energy request.

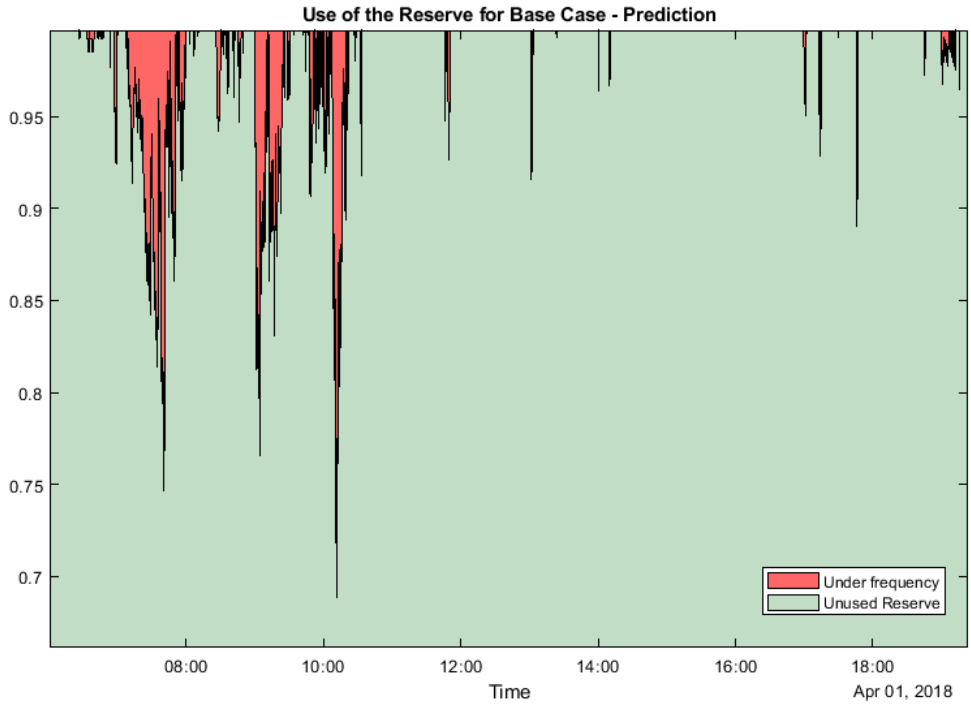


Figure 16: Prediction step: Share of reserve used for under-frequency deviation.

From this visualization it can be seen that during operating hours, the reserve is practically never used over the 30% of its value actual. One key output to acknowledge is that this reserve can be greatly decreased thanks to the HSS, and increase in output production could change significantly the economical revenues of the plant.

From the prediction phase it is extracted the predicted Market strategy for the DAM, used in the real time phase and shown in Figure 17. The norm used foresees that the energy accounted for one hour (e.g. 10AM) sums up the energy sold until the beginning of that hour (from 9:00am to 9:59AM).

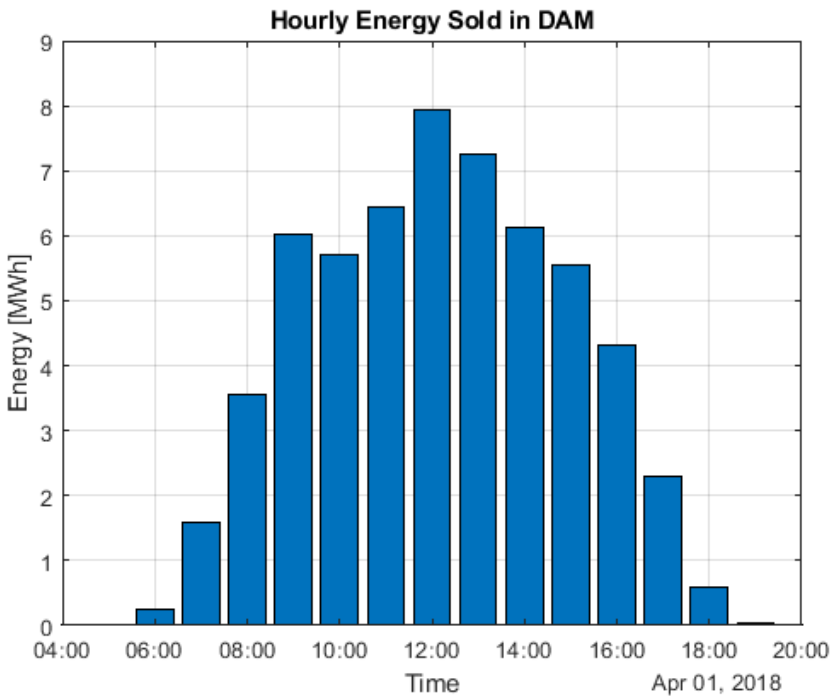


Figure 17: Prediction step: Hourly Energy for DAM.

**Real Time**

The real time phase presents a greater variability of the solar resource, as shows Figure 18

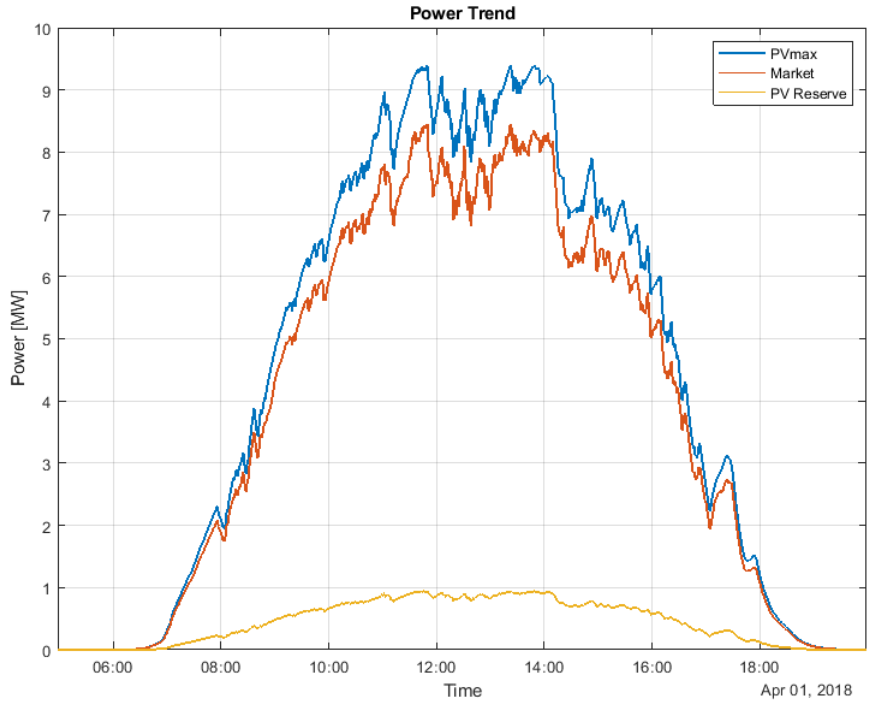


Figure 18: Real time step: Power trend over the day.

In the real time phase can be appreciated the market energy deviation due to forecast error, distinguished case by case as explained previously and synthesized in Figure 1. In Figure 19 is shown the result of the Base Case scenario, highlighting favourable and unfavourable deviations for the electrical system.

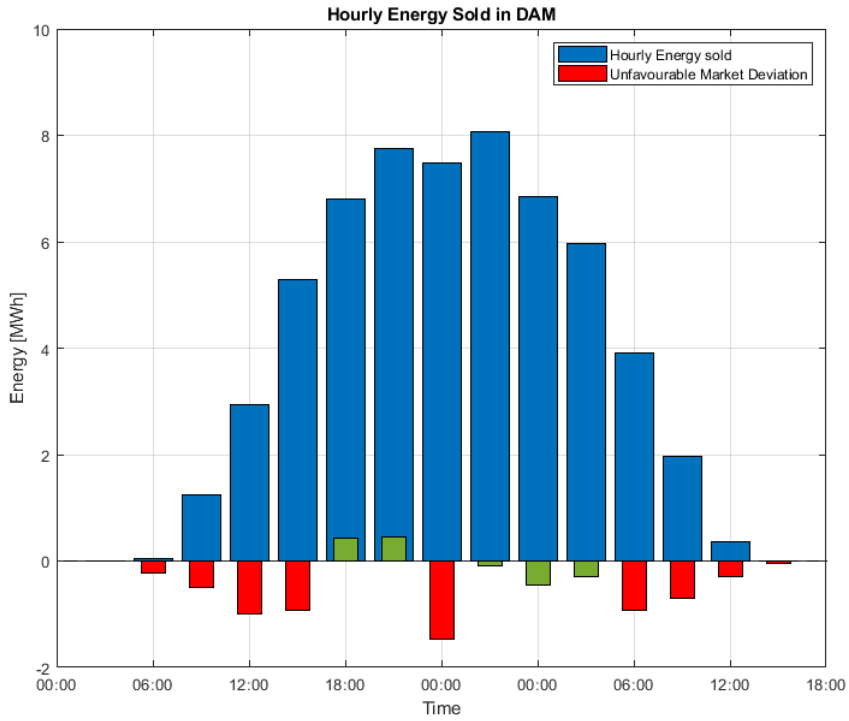


Figure 19: Real time step: Hourly Energy sold in DAM

It is meaningful to observe that any imbalance that is numerically negative, even if favourable for the electrical operator, represents a loss on the expected plant income, and therefore should be minimized. The primary aim of the HSS is to reduce this negative imbalances and maximize positive imbalances that represent (in any case) an increase in the predicted profit. At the same time, and in the limit of the economical operational benefit, the HSS optimization aims to reduce unfavourable deviations.

## 6.2 HSS Implementation

### Prediction

The optimization is here supplied with the same input data that in Section 6.1: this time the optimized HSS offers larger possibilities of flexibility. In Table 4 is presented the storage system calculated by the the optimization.

Table 4: HSS Prediction: Storage optimization output.

| HSS IMPLEMENTATION: Prediction | | | |
|---|---|---|---|
| | Battery | Flywheel | Unit |
| Rated Capacity | 518.1 | 32.0 | kWh |
| Rated Power | 971.7 | 255.9 | kW |

In Figure 20 is visible how the PV Reserve and the energy sold in the Market are greatly affected by the implementation of the flywheel and the battery.

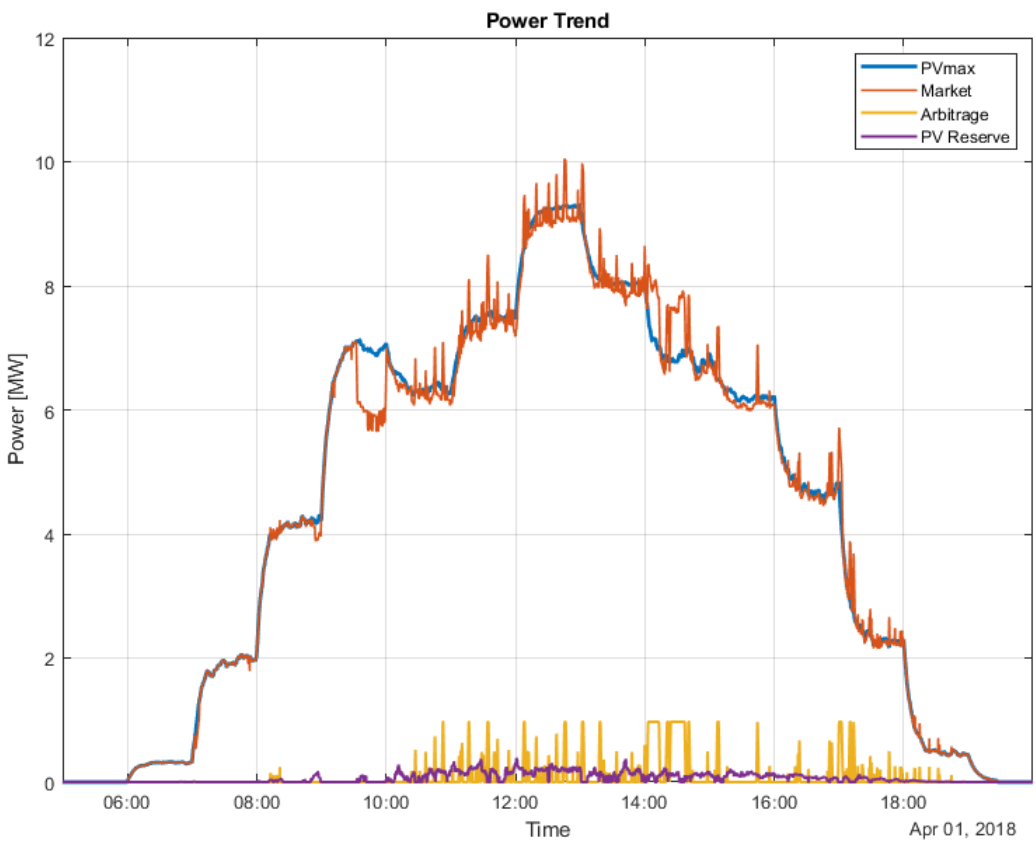


Figure 20: Prediction: Power trend over the day with HSS.

In particular, the reserve that has to be provided proportionally to the instantaneous power produced by the PV plant, is not anymore supplied solely by means of the MPPT, but main part of it is provided by the energy contained in the charge the storage systems. As it is possible to observe better from

Figure 21 the Energy sold in the Market is larger in every hour of the day, apart from time slots of the 10AM (9:00AM-9:59AM) and 11AM (10:00AM-10:59AM). In particular 10Am slot precedes the bidding time-range: during this time the HSS has to be charged in order to be able to withstand the worse under-frequency deviation for a period of 30 minutes (especially the battery).

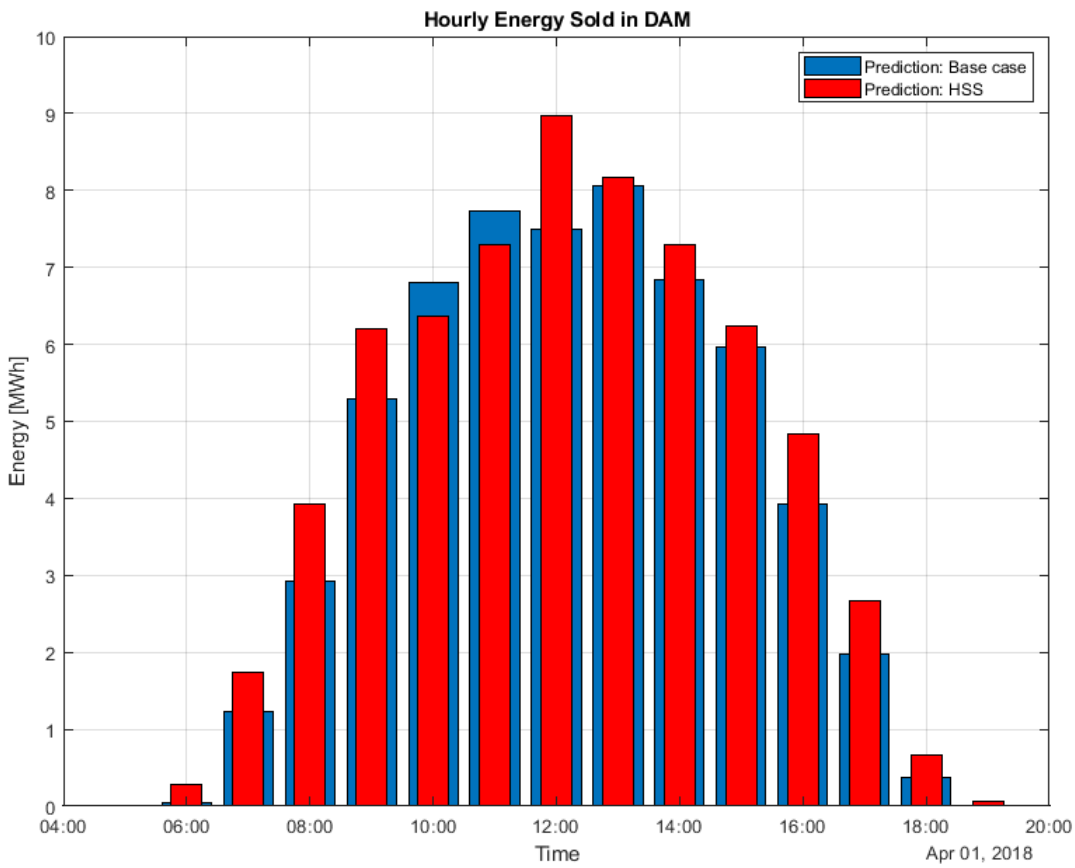


Figure 21: Prediction: Hourly Energy for DAM, comparison with Base case scenario.

The SoC evolution of the battery in particular is observable from Figure 22, while Figure 23 shows the Flywheel Energy trend.

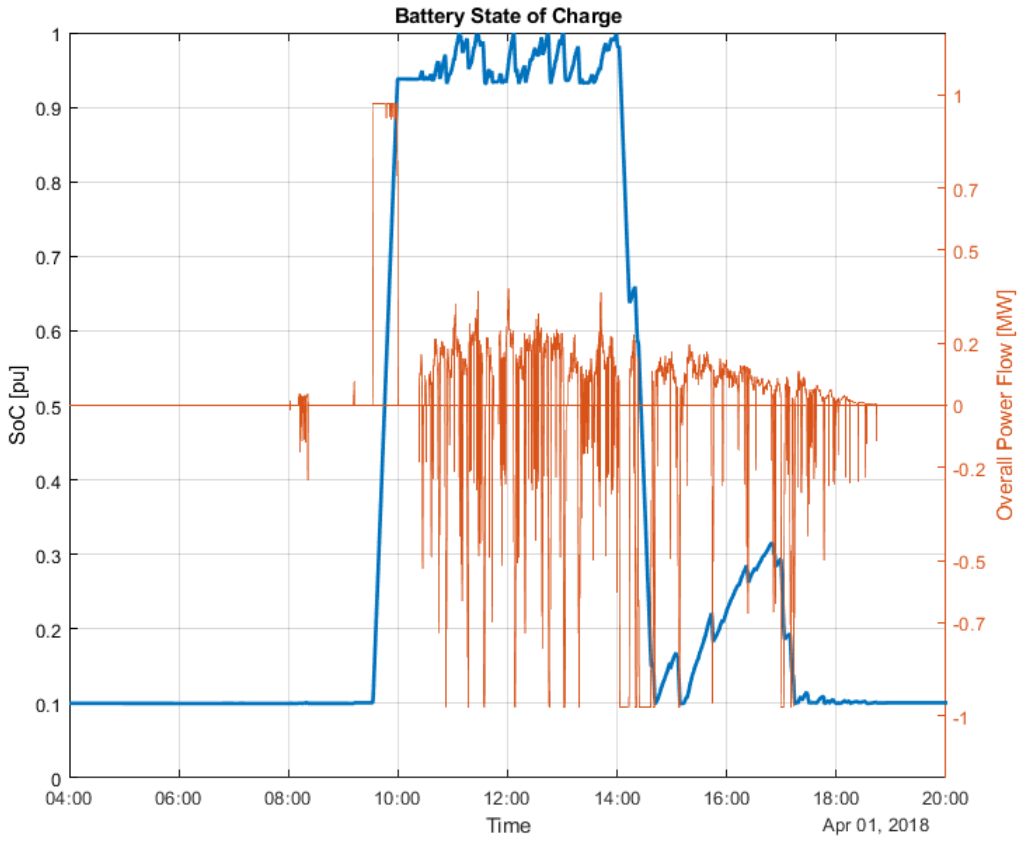


Figure 22: Prediction: SoC of the Battery throughout the day vs. Power Input Output.

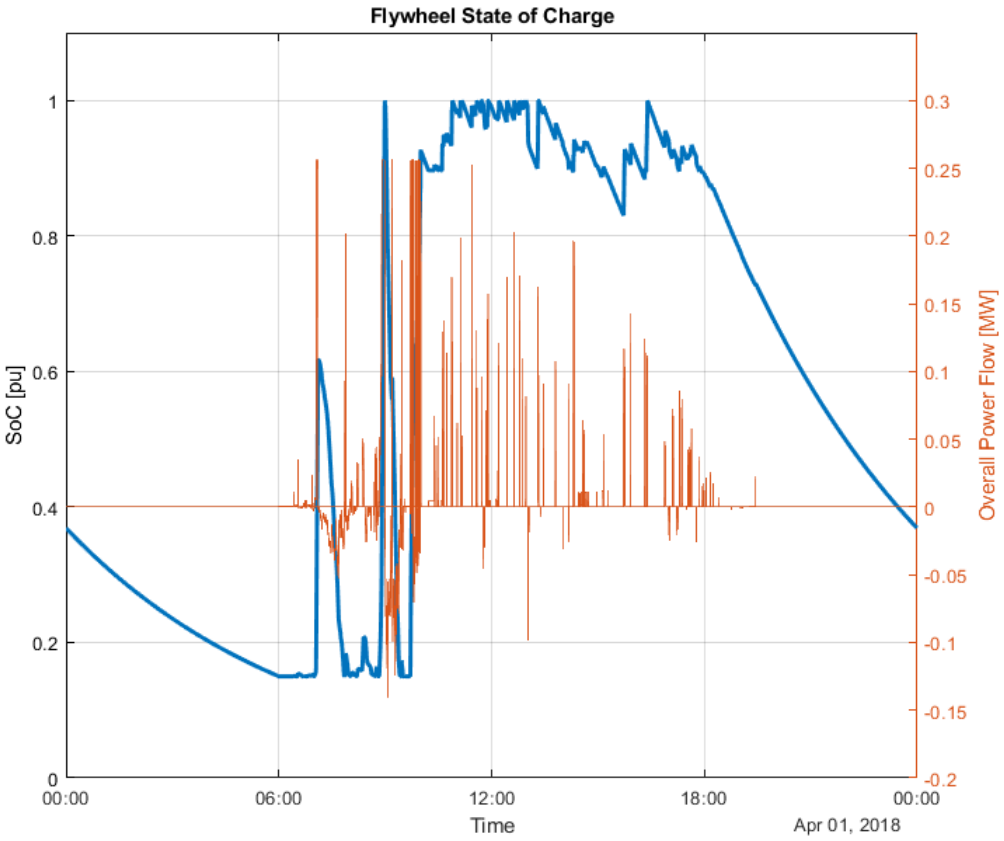


Figure 23: Prediction: SoC of the Flywheel throughout the day vs. Power Input Output.

As expected, the calendrical degradation cost dependent on the mean State of charge force the operational strategy to keep the battery SoC lower when no reserve is needed. At this point is useful to observe how the system is supplying the FCR service required for the day investigated. Figure 24 shows the overall trend of the frequency deviation response.

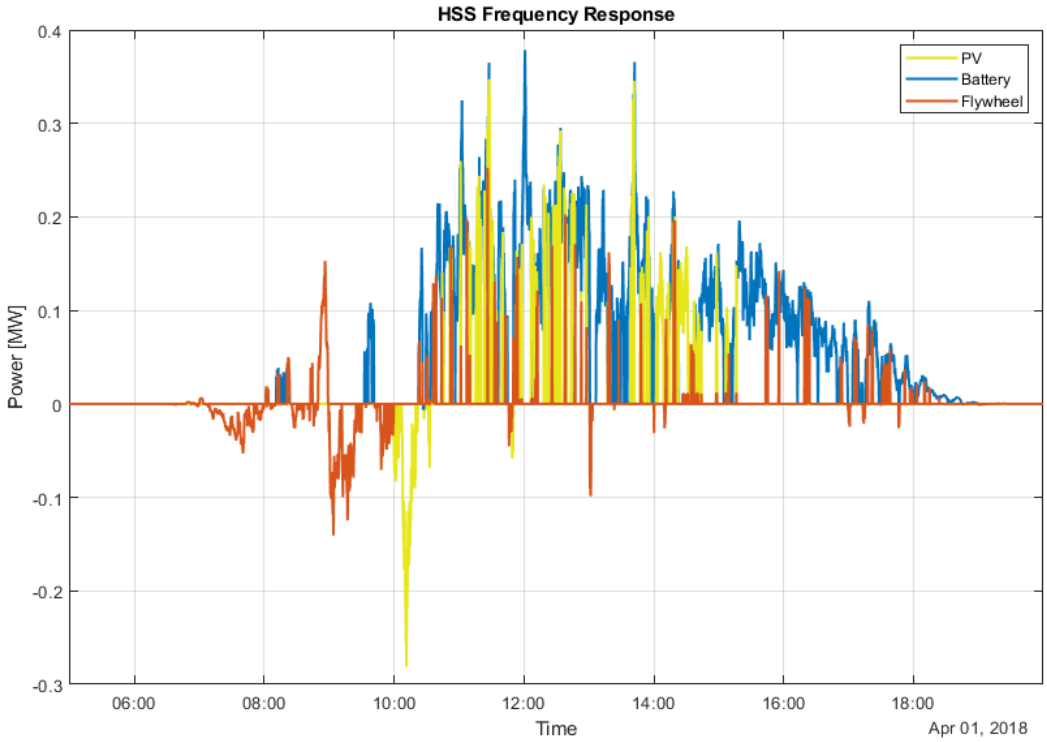


Figure 24: Prediction: Frequency deviation response by the PVPP and HSS.

Further investigation and analysis is dedicated for the Real-time phase on this matter in order to build a FCR control in the simulation final phase (see Section 6.3).

**Real Time**

In Table 5 is presented the storage system calculated by the the Optimization for the Real time phase.

Table 5: HSS Real time: Storage optimization output.

| HSS IMPLEMENTATION: Prediction | | | |
|---|---|---|---|
| | Battery | Flywheel | Unit |
| Rated Capacity | 883.1 | 32.0 | kWh |
| Rated Power | 981.4 | 255.9 | kW |

This last optimization trial is particularly slow in producing an optimal solution (from 2-6 hours depending on the type of solver used, the initial starting points evaluated and the degree of freedom

allowed for decision variables). The strategy used to accelerate this final attempt was to feed-in as initial point the ones obtained from the Prediction phase. Nevertheless, the optimal value of Battery capacity for this use case differs largely from the one obtained for the prediction step with a difference of +60%.

In Figure 25 is shown the overall power trend throughout the day, highlighting the bidding time-range.

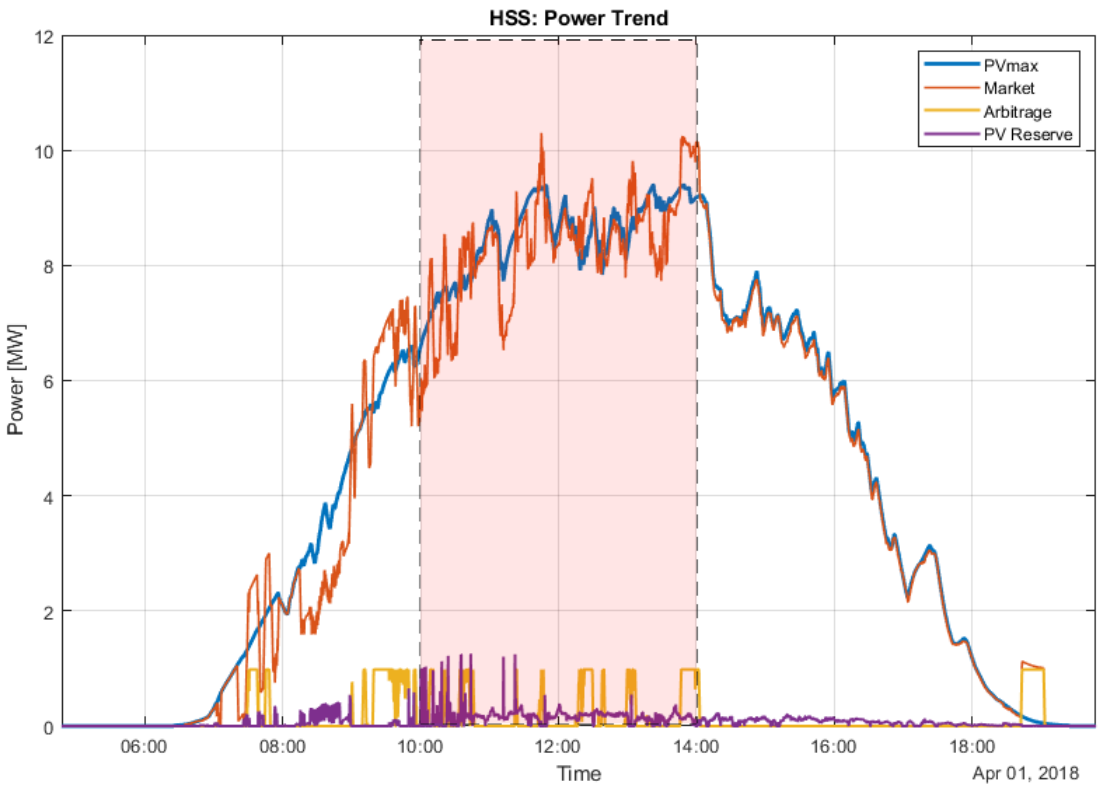


Figure 25: Real time: Power trend over the day with HSS.

Comparing the energy sold in DAM in this case (Figure 26) scenario with the one without HSS (Figure 19) is immediately clear that more energy has been sold thanks to the implementation of the storage system: the overall difference is +%10.5.

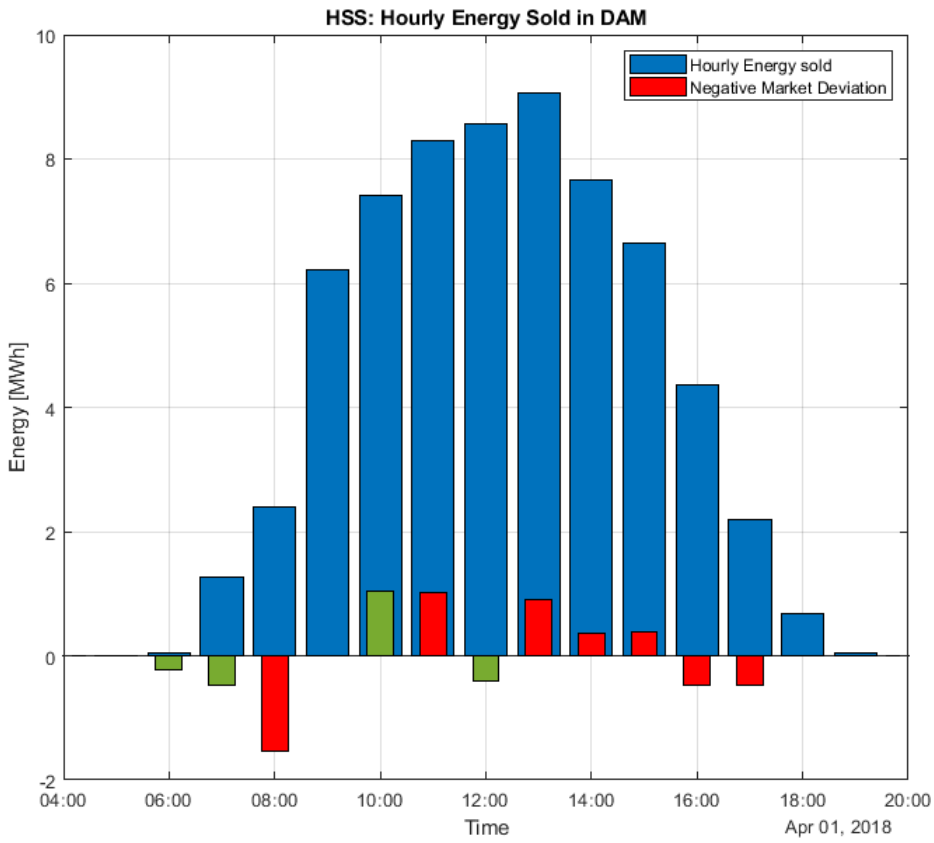


Figure 26: Real time: Hourly Energy sold in DAM.

Moreover as expected the HSS implemented reverse some of the forecast deviation: instead of less energy sold compared to the forecast, many hours are characterized by finally more energy sold. The State of Charge evolution of the Battery is shown from Figure 27, while Figure 28 shows the flywheel energy trend.

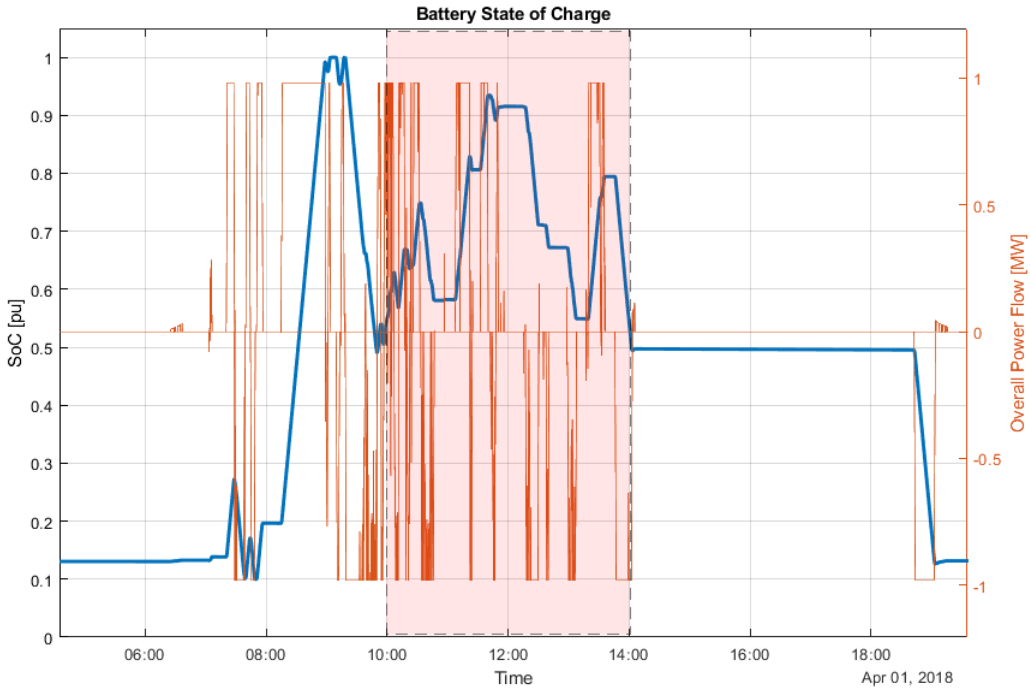


Figure 27: Real-time: SoC of the Battery throughout the day vs. Power Input Output.

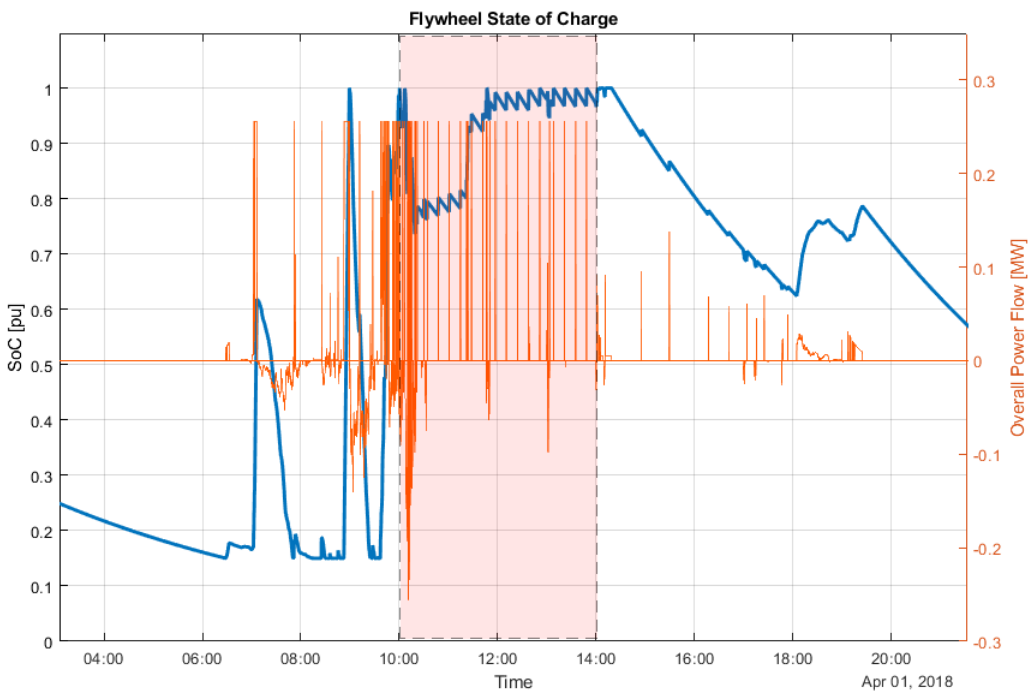


Figure 28: Real-time: SoC of the Flywheel throughout the day vs. Power Input Output.

Lastly in Figure 29 it is shown the overall PVPP frequency deviation response.

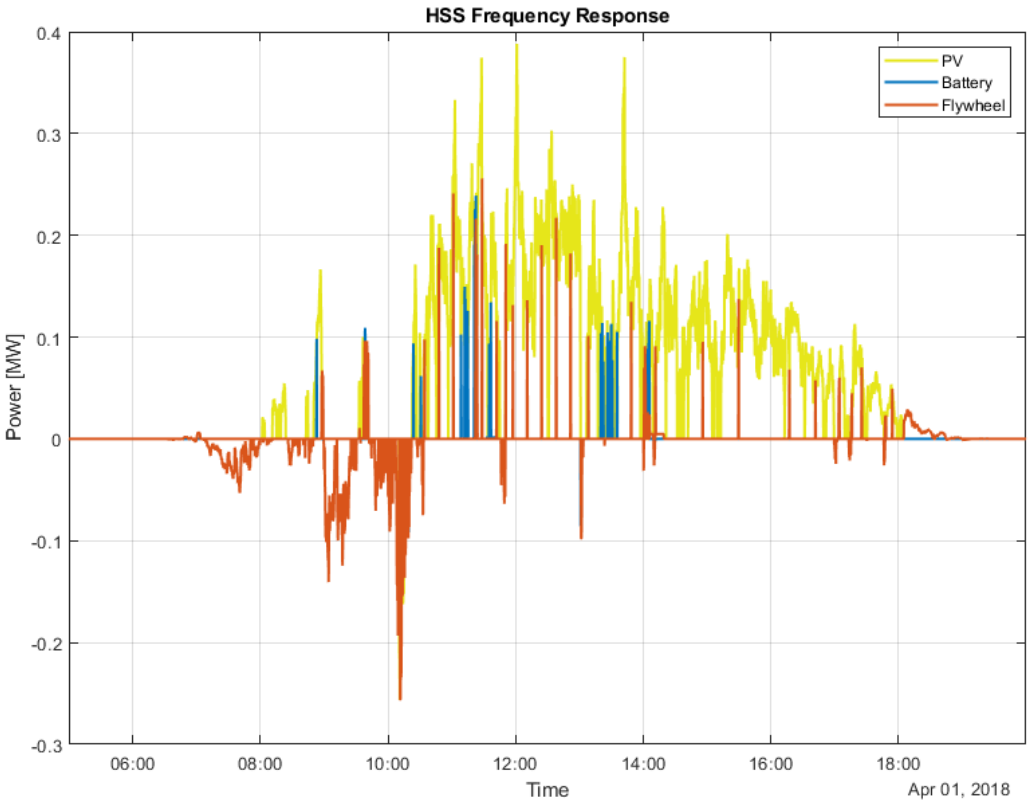


Figure 29: Real-time: Frequency deviation response by the PVPP and HSS.

### 6.3 Frequency deviation

From Figure 29 can be seen that most of the low-frequency events are solved by flywheel discharge. More specifically flywheel is providing for more than 80% of the total energy required for under-frequency deviations, while the PV power plant is injecting 15.6% of it. This result is a direct consequence of the optimization constraint settings: in Equation 29 the under-frequency events happening out from the bidding time-range are on purpose faced solely by the flywheel. Moreover as it is possible to observe from Figure 13, during bidding time the average frequency deviation requires a decrease of power output ($\overline{f} > 50Hz$), therefore low energy need have to be ensured by means of the battery and/or the PV converter.

On the other hand the PV is mainly responsible for over-frequency events ($\geq 90\%$). It is necessary

at this point to remember that the degradation cost is a virtual cost, and the optimization tends to limit the use of the storage resource if the investment for a charge cycle (in this case the cost of the equivalent degradation) is not balanced by a higher profit, finally increasing the objective function. On this regards it has to be said that with other boudary conditions, especially with less solar resource, the risk not to use over-frequency events to charge the the HSS, can compromise the energy security of the FCR: at the instant of time $bid_{start}$ the HSS could not have enough energy reserve to withstand the worst under-frequency deviation. Therefore the author opted for a control strategy that privileges and prioritize the role of the HSS to absorb from the PV output the energy required for over-frequency control.

Another important aspect to be taken in account is that the devices tend not to share the under-frequency neither over-frequency load, but to act one by one separately. In Figure 30 is shown how the over-frequency energy deviations are faced by the different energy systems.

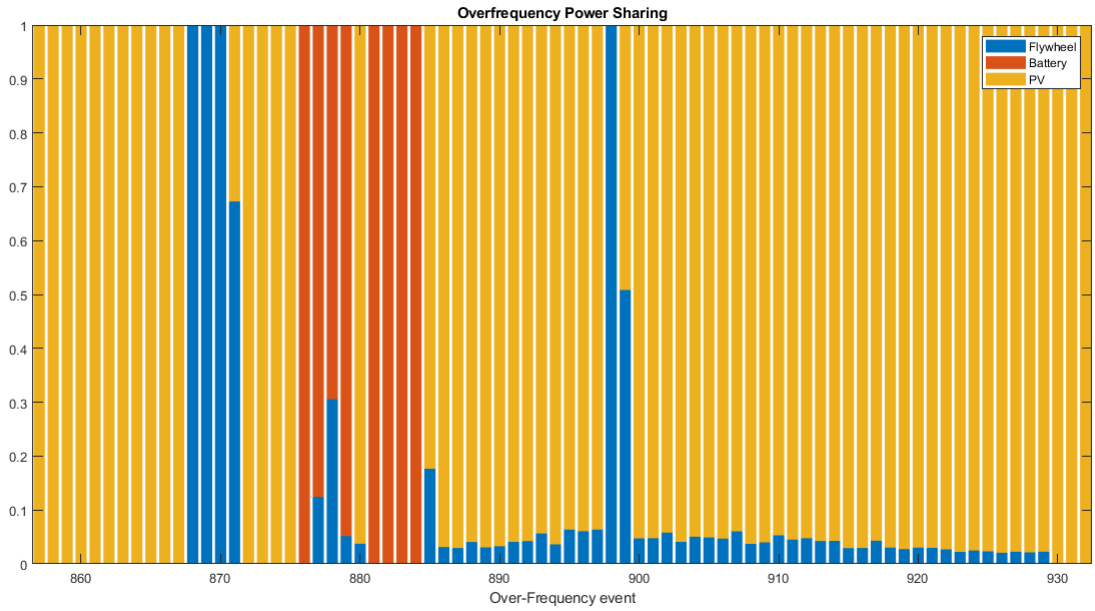


Figure 30: Real-time: Normalized over-frequency energy request shared amongst HSS and PV converter.

## 6.4 Economical Output

The yearly economical results for each case analyzed are summarized and shown in Table 6.

Table 6: Economical Comparison.

| BASE CASE | | |
|---|---|---|
| | Profit [M€] | Initial Investment [M€] |
| Prediction | 1.244 | / |
| Real Time | 1.279 | / |
| HSS IMPLEMENTATION | | |
| | Profit [M€] | Initial Investment [M€] |
| Prediction | 1.382 | 0.510 |
| Real Time | 1.401 | 0.665 |

The implementation of the HSS result in an overall increase in yearly economic gain of $+9.5\%$. It has to be once again highlighted that the profit is considering degradations cost too, representing the SoH of the battery, and taking in account share of replacement cost already in account for the current year.

### 6.5 Sensitivity Analysis

In this section is discussed how it is affected the economical result of the prediction phase optimization, varying two factors, namely the bidding time period $h_{bid}$, and the bid power reserve $P_{bid}$.

Firstly, it is investigated keeping $h_{bid} = 4$ h what is the optimal $P_{bid}$ value, not considering the minimum constraint $P_{bid} \geq 1$ MW. From the results shown in Figure 31 it is possible to conclude that the minimum requirement set by UK regulations in terms of power reserve is very close to the optimal value of $P_{bid}$ for the case study modelled, and the objective function decrease its value by only a small percentage.


Figure 31: Sensitivity Analysis: Power Reserve.

Subsequently other values of $P_{bid}$ have been taken in account with small variation in terms of profit but very large variation in terms of battery capacity: while doubling $P_{bid}$ the optimization is able to find a solution just 0.6% less profitable than the optimal, the battery size result to be more than doubled (see Figure 32). This result is in line with the fact that the battery capacity is mainly responsible for the FCR reserve, while the flywheel is not changing in size, varying $P_{bid}$ .

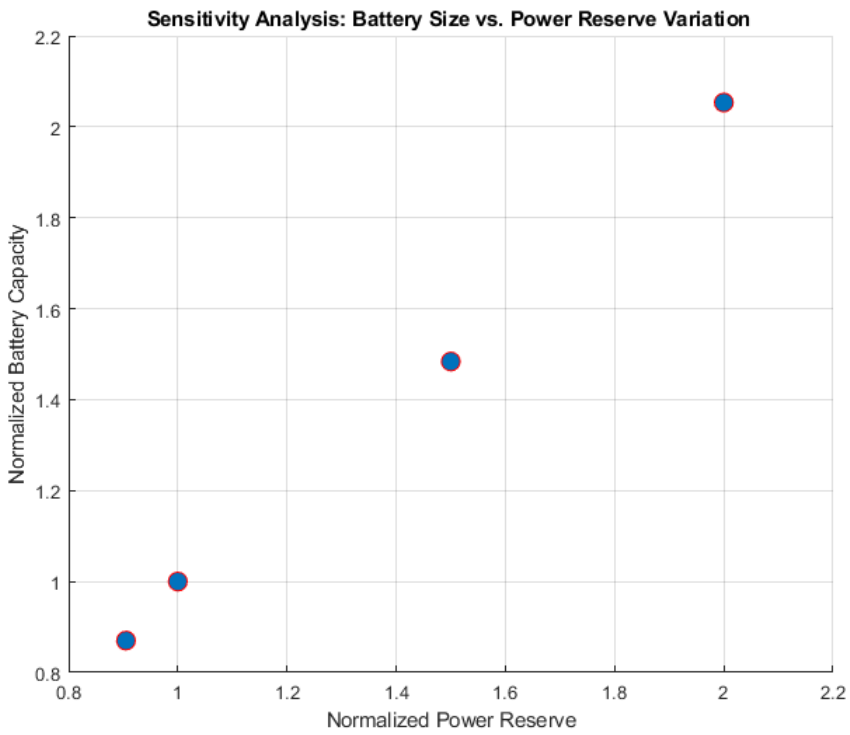


Figure 32: Sensitivity Analysis: Power Reserve.

Instead in Figure 33 it can be observed how, increasing of one unity the hour in the bidding period range, the profit is not increasing with the same trend: the tendency of the points shows that a point of maximum is approaching.

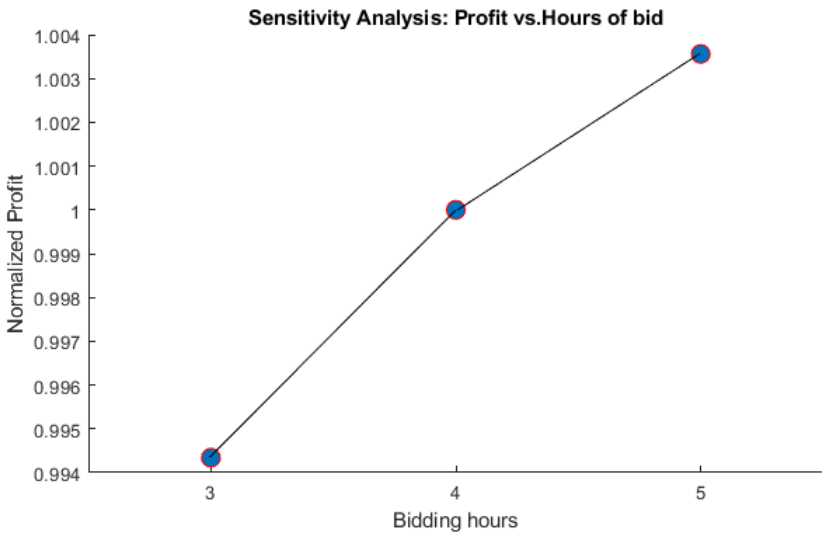


Figure 33: Sensitivity Analysis: Bidding time-range.

A conservative strategy has been chosen to select the $h_{bid}$ factor since is very likely that the profit function could decrease consistently in other days of the month due to solar scarcity out from sunniest period of the day.

It can be concluded that the variables analyzed in the sensitivity analysis are quantified as follows:

- $P_{bid} = 1$ MW;
- $h_{bid} = 4$ h.

# 7 Simulation Model

In this Section is modeled and tested a Simulink model comprehensive of the following features:

1. Battery Management System: through a linear regression model and a slow PI controller acts on battery side converter voltage, to control the State of Charge of the battery, and ensure a minimum energy level is kept for FCR;

2. Current controllers: through fast PI controllers control the current, therefore the power input and output both for the flywheel and the battery;

3. Under Over-frequency controllers: produce a current control signal that is passed to the Current controllers in order to respond to frequency deviations.

The structure of each element is described first, together with assumptions building controllers and finally results of simulations are discussed.

## 7.1 Design of Components

Firstly, to correctly model the HSS is necessary to design the devices assuming physical constraints and market options.

More specifically the Lithium Ion Battery has to be designed assuming battery cell characteristics and pack voltage in order to limit the rated current. On the other hand flywheel has to be designed in terms of composing material, in a way that the device can withstand the maximum stress given by the rotating velocity. For the same reason the rotation minimum and maximum speed have to be constrained, together with the radius of the disk and consequently a motor has to be chosen. The results of the design are shown in Tables 7 and 8.

| Battery Design | | |
|---|---|---|
| | Value | Unit |
| Series | 140 | n |
| Parallels | 880 | n |
| Pack Voltage | 504 | V |
| Pack Current C/1 | 1760 | A |

Table 7: Battery Pack Characteristics

| Flywheel Design | | |
|---|---|---|
| | Value | Unit |
| Material | Carbon AS4C | / |
| Outer Radius | 0.21 | m |
| J | 10.94 | $kg \cdot m^2$ |
| $w_{max}$ | 46 | krpm |
| $w_{min}$ | 14 | krpm |

Table 8: Flywheel Characteristics

The flywheel had to be oversized in terms of Rated Power, up to $\approx 4 \cdot P_{flywheel}$, the value calculated in the optimization because the normalized inertia was too large (the $P/E$ ratio was too small).

## 7.2 Model of the Battery

The model developed in Simulink is shown in Figure 34.

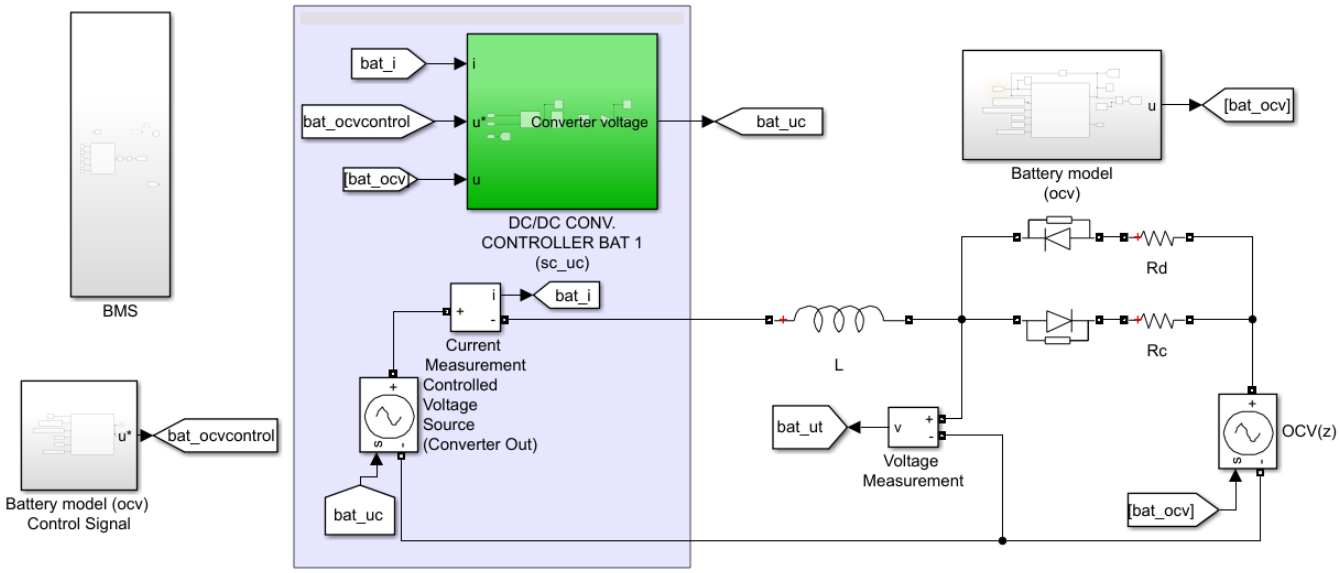


Figure 34: Overview Battery model.

The scope of the component indicated as BMS is to calculate, depending on some boundary conditions, the optimal SoC of the battery. The structure of the subsystem is shown in Figure 35

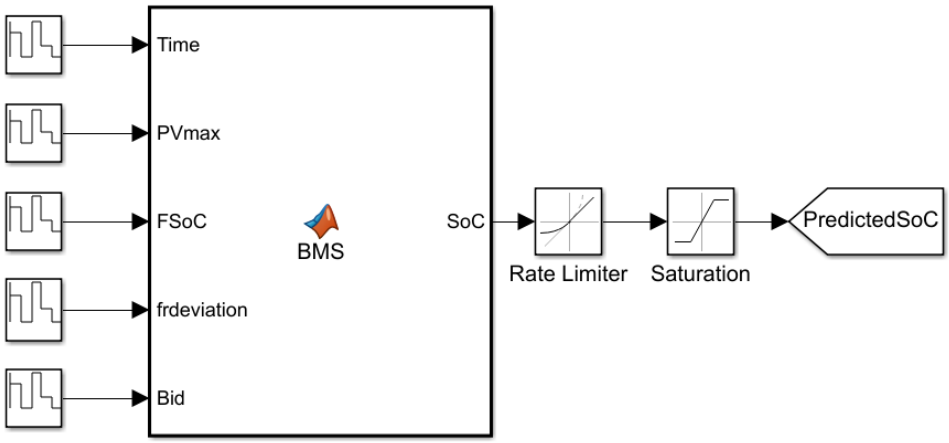


Figure 35: Battery Management System: SoC Prediction.

The Matlab Function block uses a linear regression model built starting from the Optimization results obtained in the HSS Real Time Implementation. The output is therefore filtered through a rate limiter that limits the change in SoC as a function of the rated power of the battery. The saturation block saturate the control signal to the maximum and minimum value admissible of SoC level. The control signal is sent to the "Battery model OCV" subsystem that, through an interpolation computes the value of Open Circuit Voltage "$bat_{ocvcontrol}$". This value is the control signal for the voltage controller described in Section 7.3

### 7.2.1 Linear Regression Model

In supervised learning, the scope of a regression is to infer a function from labeled training data consisting of a set of training examples [47]. In this case the training data are the variables input (on the left) in Figure 35 and the regression function is built in a way it can predict effectively the optimal SoC of the battery calculated through GAMS optimization. In this process, the aim is to make use of the GAMS optimization result to train a function able to set in real time (continuously fed by incoming input data) an optimal battery charging-discharging behaviour. In this sense it can be said that the controller developed is an online controller, since all the input data chosen to build the regression function are easily extracted by the same simulation, since all the variables are known.

The resulting prediction of the Battery State of Charge, for the day investigated is shown in Figure 36 compared to the optimal value calculated every 15 seconds by GAMS optimization.

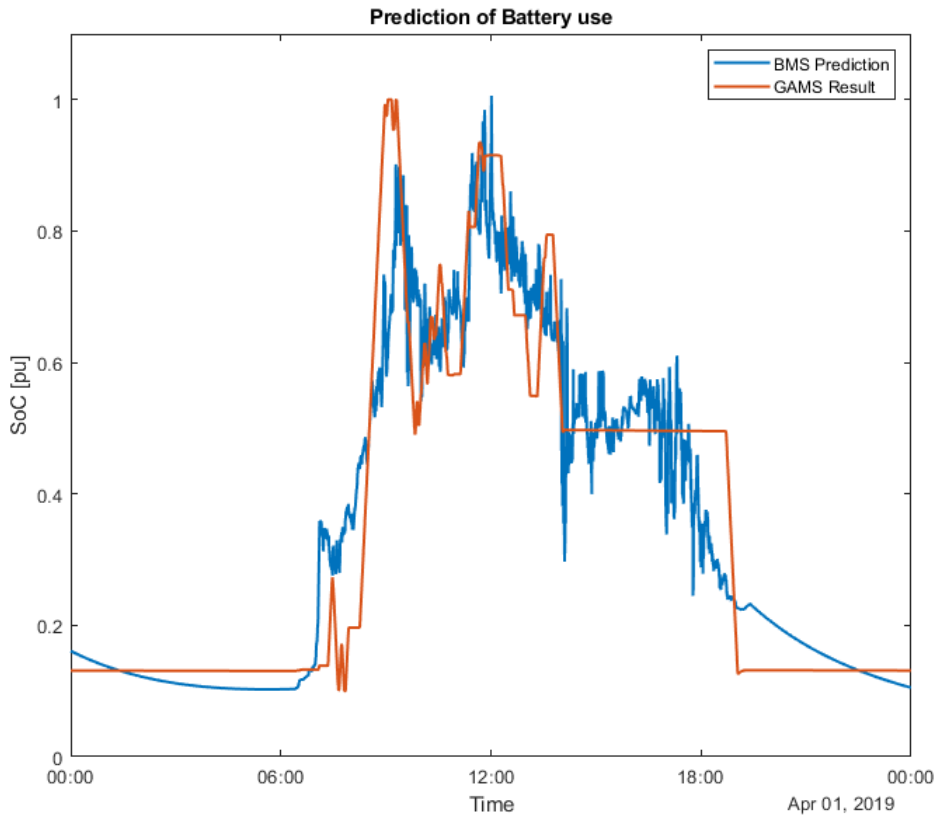


Figure 36: Battery SoC Prediction: Linear regression output vs. Optimal SoC.

The linear regression is set to contain an intercept term, linear and squared terms for each predictor, and all products of pairs of distinct predictors: in total the equation is formed by 16 terms. It is important to highlight that this regression function is effectively predicting the Battery State of Charge solely because the Training Data is the same as the Test Data. The linear regression should fed by many input Training days of battery use to be able in a second step to test a new Test day and effectively verify the capabilities and the effectiveness of the regression model. For limited time resource it was not possible to create many Optimization results, and the author preferred to limit the analysis to make use of the data obtained, mainly to describe a process strategy rather than an accurate numerical solution. Following, in Figure 37 are shown the main effects of the input factors on the predicted State of Charge.

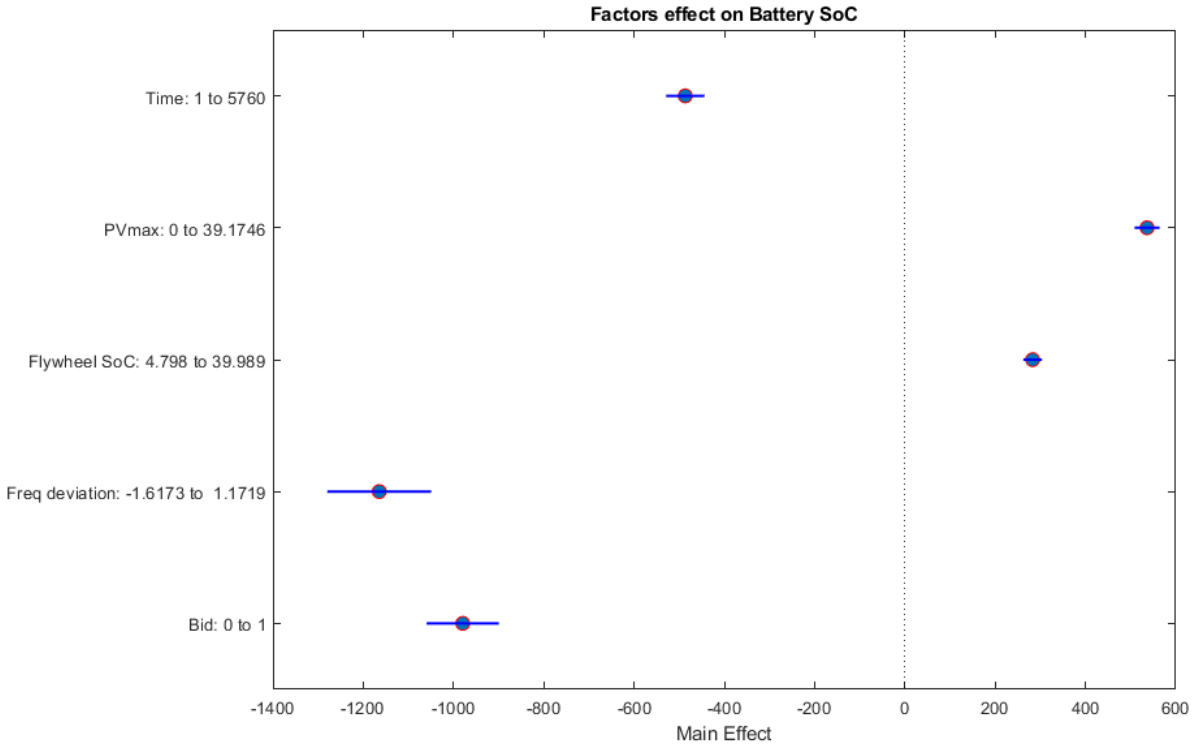


Figure 37: Battery SoC Prediction: Expected change in output given change in input factors.

The circles show the magnitude of the effect and the blue lines show the upper and lower confidence limits for the main effect. For example, if the flywheel reaches its maximum SoC, the expected prediction increases by 250 kWh compared to when the flywheel is completely discharged, given all else is held constant. Once again, it is possible to see how the confidence interval of some factor is very large, and the dependency with the output prediction is definitely distorted. The prediction would benefit from more input data: in this case the author expects less effect from factors such as the frequency deviation.

## 7.3 Voltage Controller

The Voltage Controller accepts as an input the error between the actual value of the OCV of the battery (indirect measure of the Battery SoC) with the optimal value calculated by the BMS block. If the error is positive, means that the battery should be charged to increase its energy content. Figure 38 shows the controller scheme.

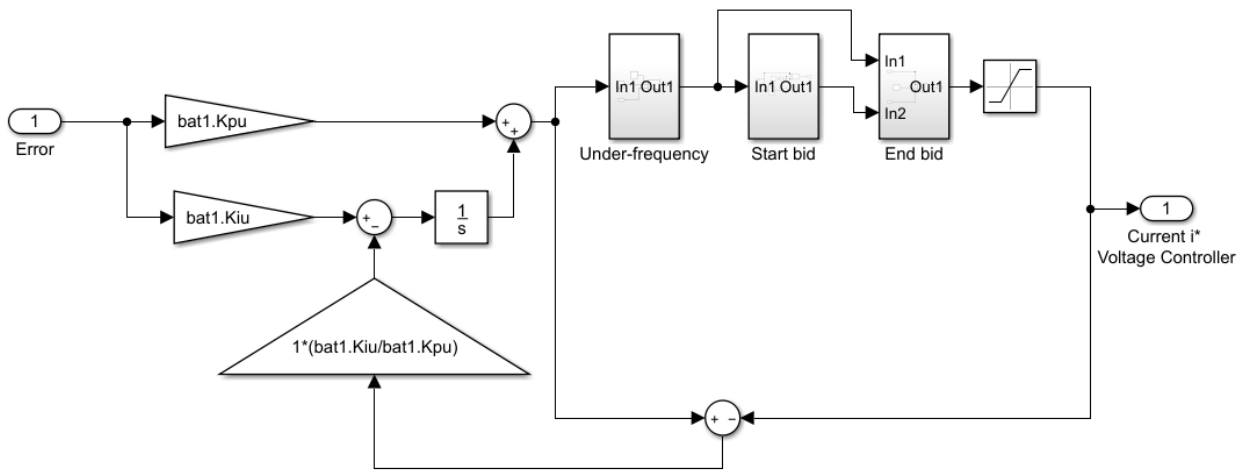


Figure 38: Voltage controller overview.

The controller is equipped with a anti-windup control to limit undesired effects from large change in set-point and consequent significant error derived by the integral term. The groups of subsystems on the right have two main aims:

1. In case of under-frequency event, and the battery is responsible to provide the equivalent energy, the chargin-discharging behaviour to follow to optimal SoC is automatically nullified;

2. In case the operations happen inside the bidding time-range, the voltage controller is constrained to a saturated current output equals to 10% of the rated current.

The first aim is necessary in case a sudden under-frequency event happens and the optimal SoC requires to charge the battery: the two signal are in contradiction and the result has been tested to be not accurate, even if the Voltage controller current is constrained to low values. This is logical since the current requested by the frequency deviations are usually in the range of 5-10% of the rated power of the battery. The second aim has been thought to limit the change in SoC once reached the minimum value to provide FCR: in this way, even if the prediction could output a lower signal of SoC (mainly due to prediction error), the effect of the control signal is slowed down by a smaller battery reaction in terms of current signal. The code that exemplify the switching blocks contained in the subsystems is shown in 10.1

## 7.4 Current controller

The current output from the voltage controller is summed up with two other inputs as shown in Figure 39, the Under-frequency and Over-frequency current input, consequently an error is calculated through the use of the actual current in the battery pack.

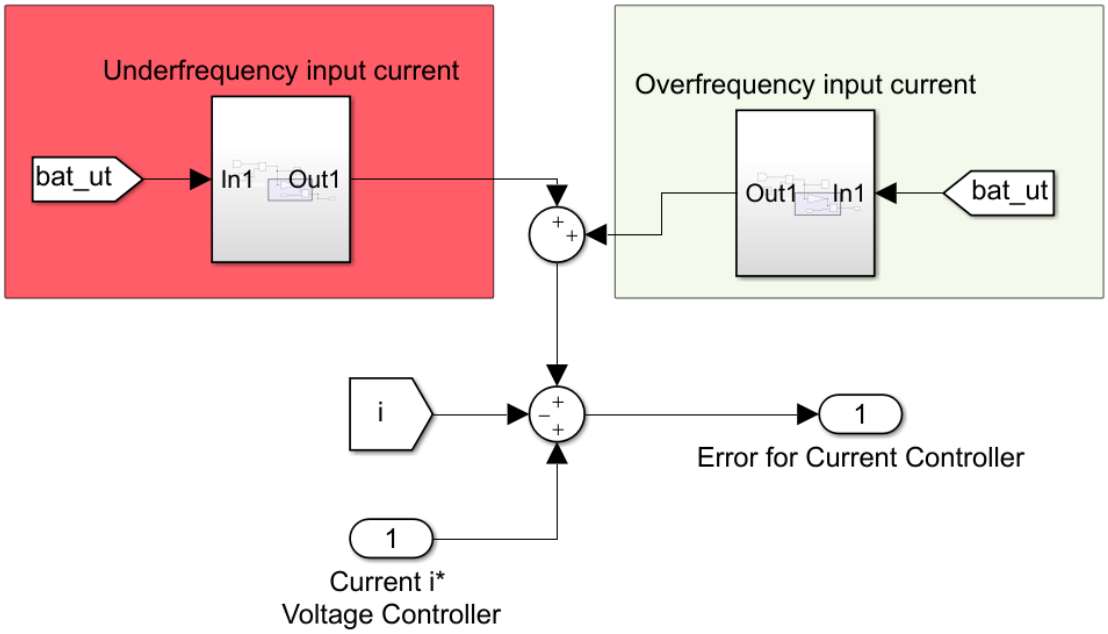


Figure 39: Calculation of the error for the Current Controller.

The subsystems in red and light green simply receive the energy requested for frequency deviation from the main Frequency deviation controllers (described in Section 7.8) and through the value of the battery voltage output the value of the current to be produced in order to obtain the energy requested.

In a nutshell, the output from the DC/DC Converter Controller just examined is the voltage to be produced by the converter $u_c$, on the battery side, in order to comply with the current controller (fast reaction, under-over frequency control) and the voltage controller (slow reaction, optimal predicted SoC).

## 7.5 Tuning of the PIs controller

The tuning of the PI controller is aimed to minimize the current injected or ejected from the battery, while being enough reactive to increase the SoC in order to provide reserve throughout the Bidding

period. In fact, even if the model developed in Section 7.2.1 predict the overall trend of SoC with an acceptable level of precision, the noise in the signal is quite large.

At the same time, when the reserve is needed, the current injected in the battery has to be large enough to charge the battery in time and comply with the minimum reserve requirement calculated in the optimization.

## 7.6 Model of the flywheel

The flywheel is modeled starting from the following set of equations:

$$E_{tot} = \frac{1}{2} \cdot J \cdot \left(\omega_{max}^2 - \omega_{min}^2\right) \tag{55}$$

$$P = T_{electrical} \cdot \omega(t) \tag{56}$$

**Losses**

Losses were modelled in a way that a constant Torque $T_{losses}$ is applied to the electrical Torque. The losses are assumed to be proportional to the actual velocity of the Flywheel: the power loss is in fact modelled as follows:

$$P_{losses}(t) = T_{losses} \cdot \omega(t) \tag{57}$$

The value of $T_{losses}$ was calculated given the parameter used in the optimization of 15% loss in state of charge (hourly). Using the Equation 56 it was calculated the final velocity that the flywheel should have, under $T_{losses}$ only (that means 15% of energy loss).

$$E_{loss}(1h) = \int_0^{1h} P_{loss}(t) \cdot dt \tag{58}$$

Substituting in the Equation 58 the expression of the $P_{loss}(t)$ is calculated the value of $T_{losses}$. In Figure 40 is shown a 1 hour test of the flywheel subjected to a null load, starting from the maximum level of SoC.

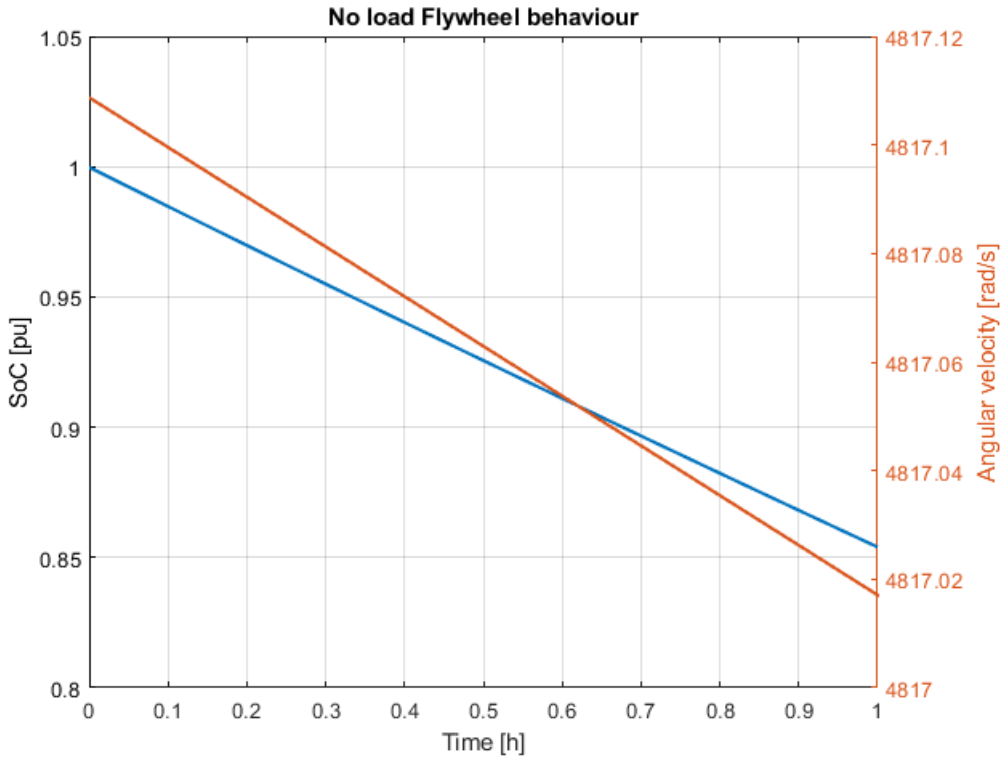


Figure 40: Flywheel losses: after 1 hour the State of charge is near to 85%.

## 7.7 Control of the SoC

A simple control method is used to avoid that the flywheel is discharged when the $SoC_{min}$ level is reached and charged over the $SoC_{max}$. The Matlab function is shown in 10.2. No controller is used to control furthermore the State of Charge of the flywheel, but a deterministic approach based on main results from the optimization GAMS results. In Figure 41 it is shown how the deterministic strategy has been developed in Simulink environment.

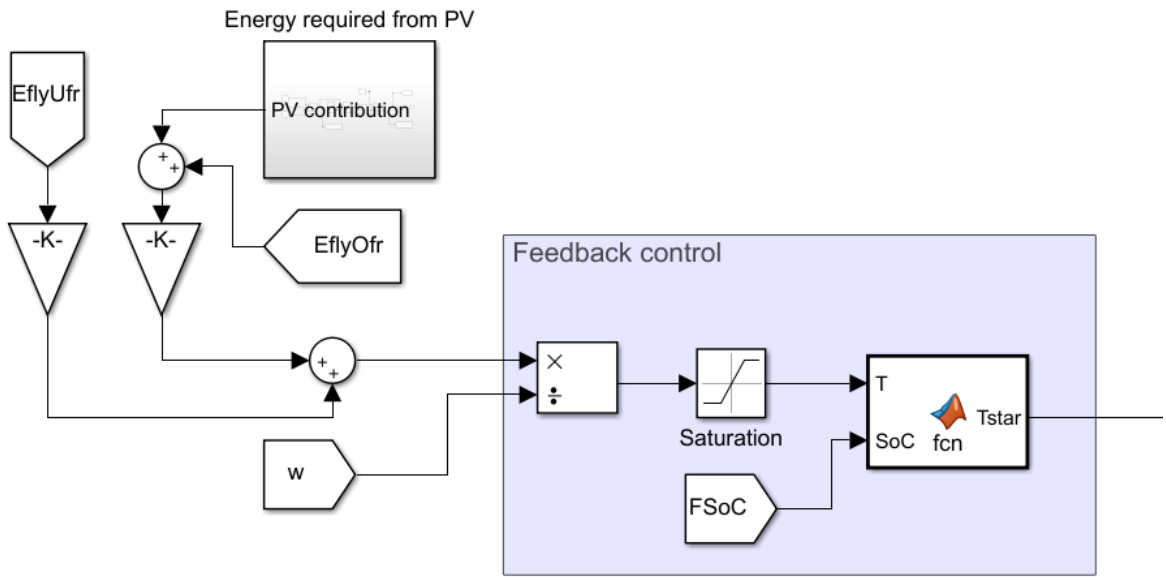


Figure 41: Flywheel deterministic control overview.

The energy requested to the flywheel for under-overfrequency control is summed up with the energy contribution directly from the PV: the subsystem has two main objectives:

1. Charge the flywheel when the $SoC_{min}$ is reached with a small quantity of energy, quantity set to be 0.2kWh (50kW for each time step of 15s);

2. If in bidding time-range, the flywheel has to maintain a specific $SoC_{BIDmin}$, extracted from GAMS optimization output to be able to correctly react to sudden under-frequency events.

As described for the battery control, also the flywheel injection of energy is stopped when discharge is required.

## 7.8 Frequency sharing control

The controllers responsible to share the frequency deviation response (positive and negative) upon the different devices are quite similar in terms of strategy, but they differ in one aspect:

- As a result from the operational GAMS strategy, it was observed that the under-frequency response is ensured mainly by the HSS only, while the over-frequency relies on the PV control.

As a logical strategy the author decided to assign under-frequency response to HSS only and include the PV contribution in the over-frequency controller.

In Figure 42 is shown the control subsystems with their equivalent output.

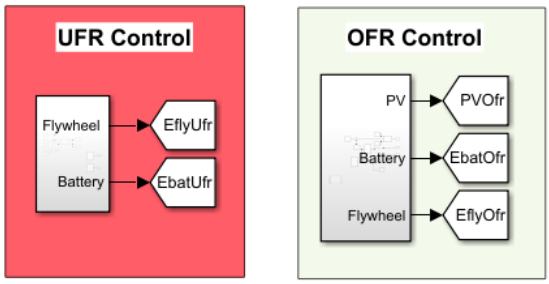


Figure 42: Frequency controllers overview.

The common strategy for the controllers is set through the use of several switching blocks as can be seen in Figure 43, showing th Over-frequency control scheme.

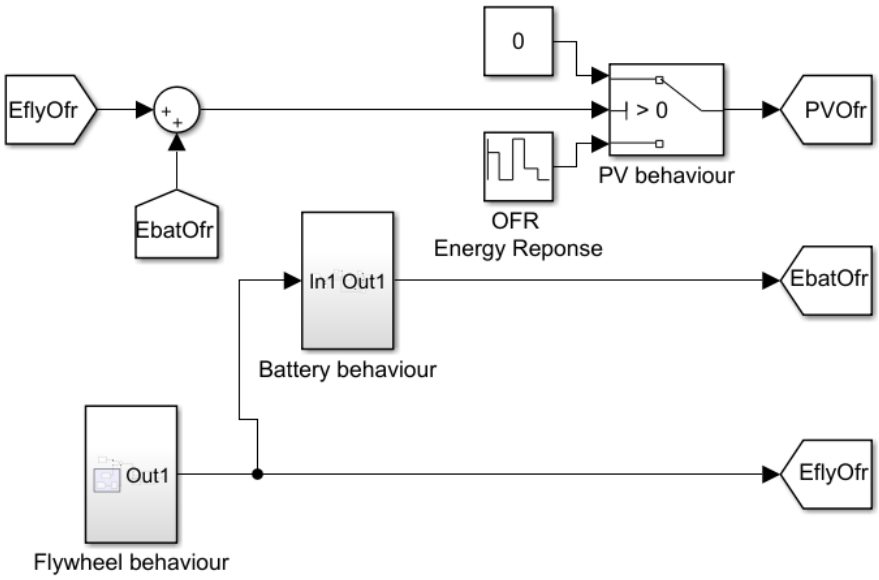


Figure 43: Over-frequency controller overview.

By a way of example is shown the control for the over-frequency flywheel response in Figure 44.

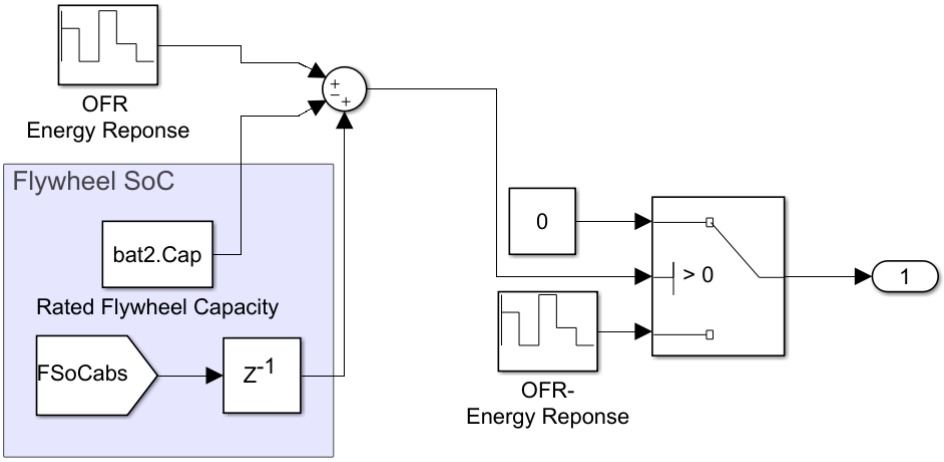


Figure 44: Over-frequency controller flywheel behaviour subsystem.

In this case the Over-frequency response is passed firstly to the flywheel control, that checks whether the injected energy would not charge the flywheel over its rated capacity. If the condition is not verified, and the flywheel cannot bear the energy input, the reponse is assigned in a second stage to the battery control, that presents the selfsame control illustrated in Figure 44 for the flywheel. Finally if none of the two device is accepting the over-frequency energy input, the energy is assigned to the PV controller (MPPT not modeled in this study).

The under-frequency controller acts in an equivalent way.

## 7.9 Simulation results

The model described previously is finally fed with the same input data used for the GAMS optimization to test the capability of the prototype of EMS described. An effective result should imitate the GAMS optimal operation result, but it has to be highlighted that the Simulink Model lacks of one feature that is present in the GAMS optimization. In fact, the battery controller is able to provide an optimal SoC on average and PFC, but the arbitrage operational strategy is not built in the model. This added feature would require another layer of control, to be coupled with the Frequency response on the basis of a *Priority algorithm*, as already developed in literature [48]. For obvious reasons the frequency control should have in fact a higher priority over the market arbitrage control.

The results of the simulation are shown for each device, highlighting overall differences with GAMS

results.

**Flywheel**

In Figure 45 it can be observed that the average value of the flywheel SoC is higher than the one calculated by GAMS optimization (see Figures 28): the FCR strategy is in fact prioritizing this device charging it when an over-frequency event occurs (see Figure 46).

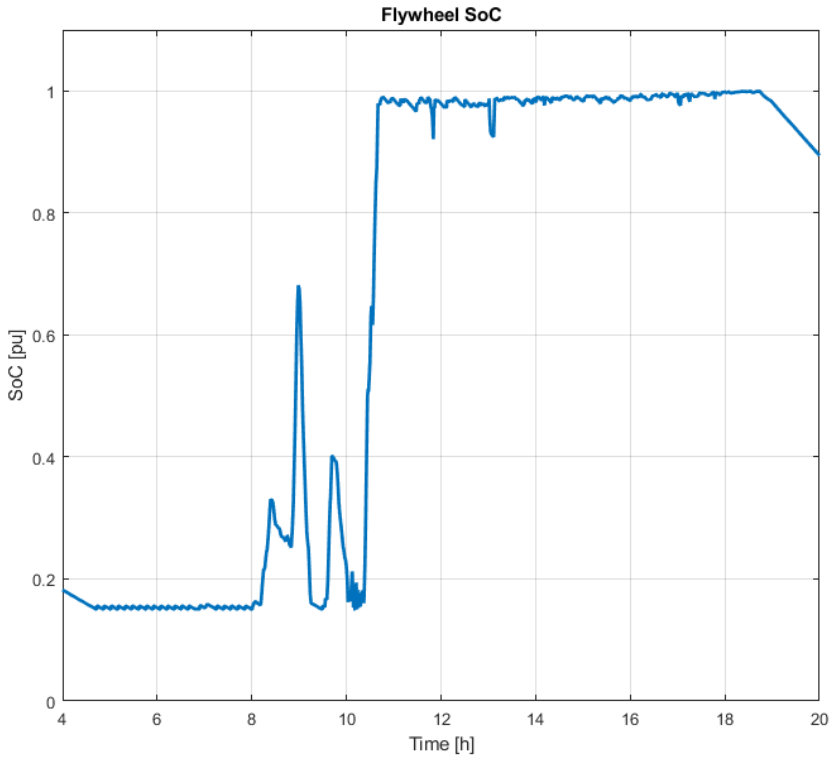


Figure 45: Flywheel simulation State of Charge.

Results show that the flywheel has to be recharged in the early morning period. A problem emerges since no PV production is available: it is therefore necessary to charge the flywheel from the grid to maintain the minimum level of SoC.

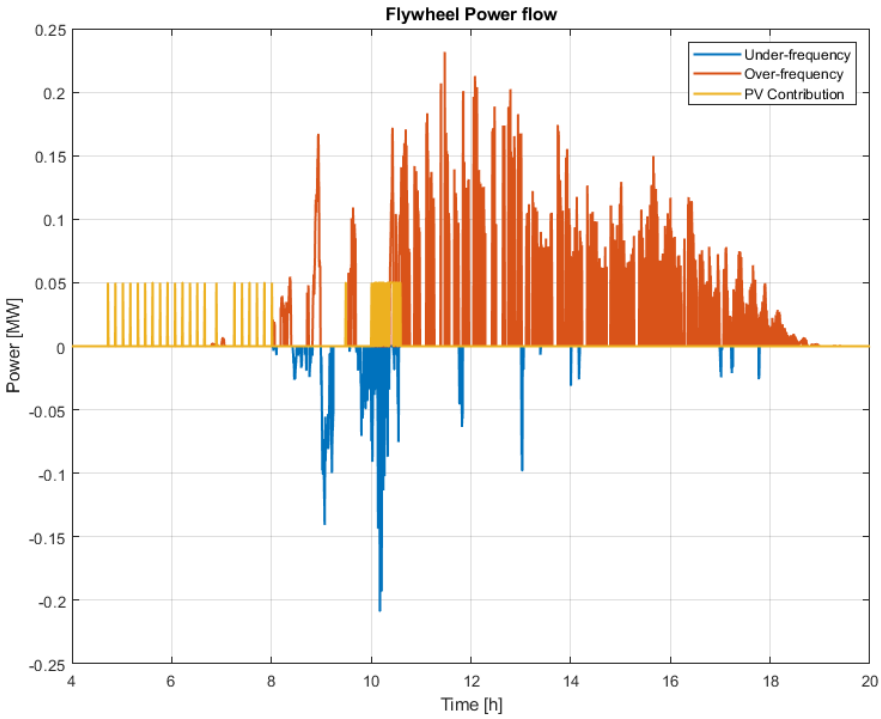


Figure 46: Flywheel simulation power flow.

**Battery**

In Figure 47 is also visible that the battery slightly differ from the trend calculated in GAMS optimization: also in this case the over-frequency control increase the average SoC of the battery, leaving the Storage device with a higher energy content.

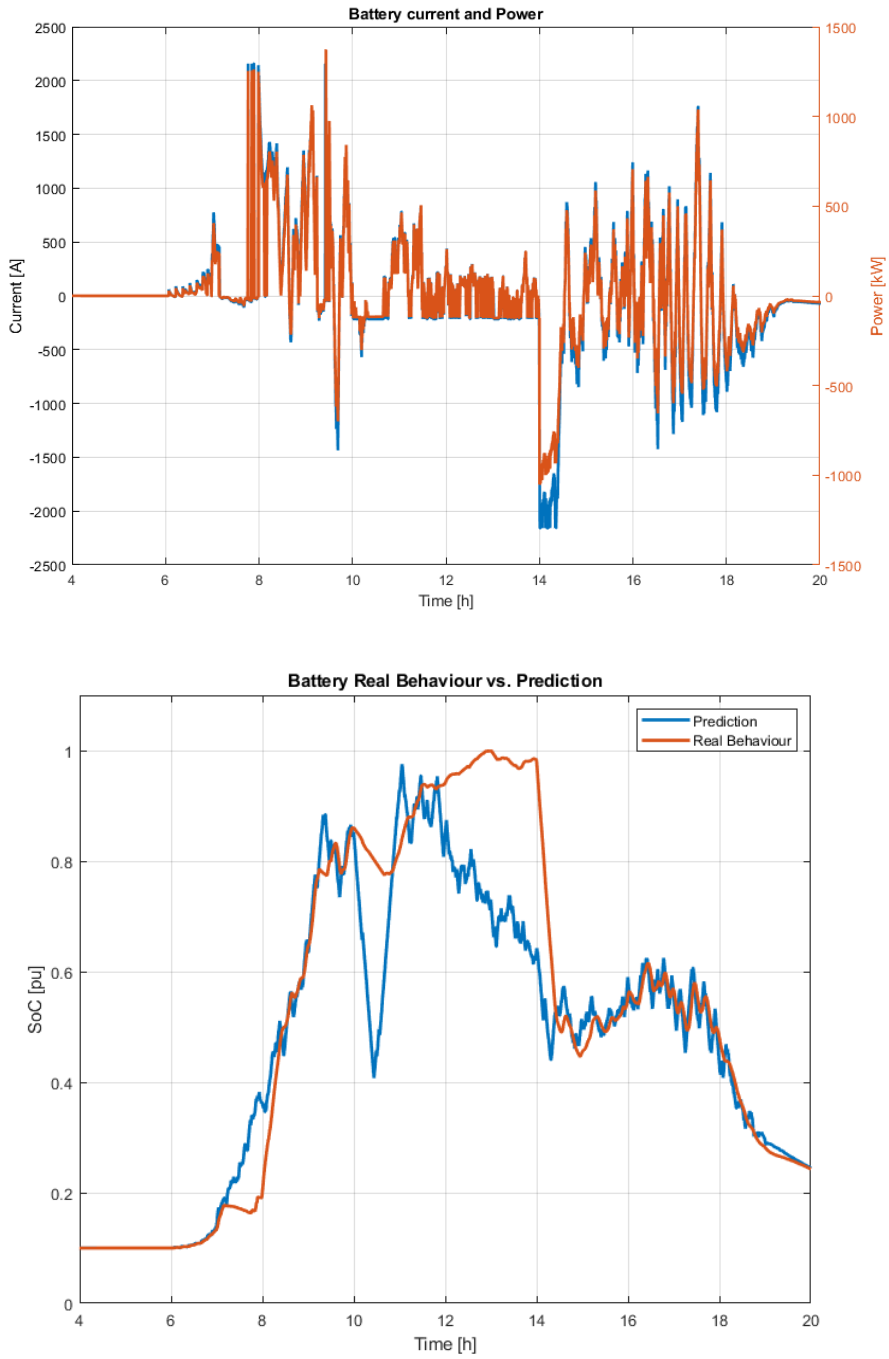


Figure 47: Battery overall behaviour.

**Frequency deviation Sharing**

At this point it is useful for the purpose of the analysis to observe how the over and under frequency deviation are shared upon the different devices. Flywheel and Battery are responsible for most of the over-frequency control apart from the period of time in which both the device are completely charged

(around 1PM, see Figure 48)

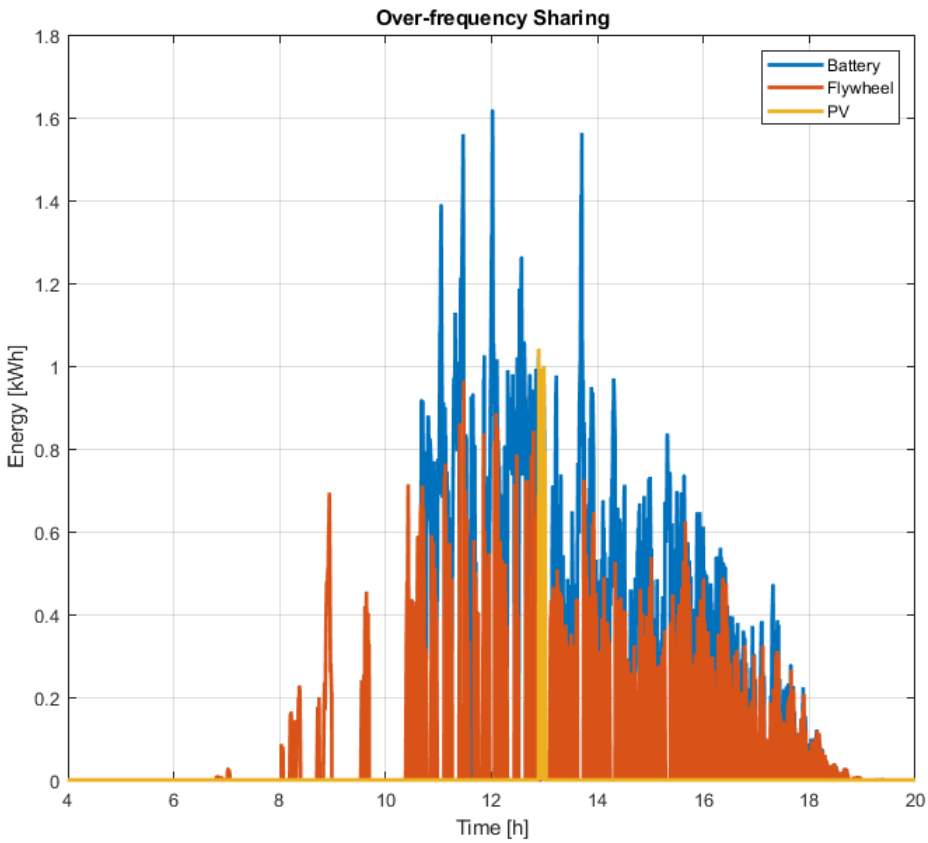


Figure 48: Over-frequency sharing strategy.

Instead under-frequency control is mainly ensured by flywheel apart from the early morning period in which the flywheel has no energy available, see Figure 49.

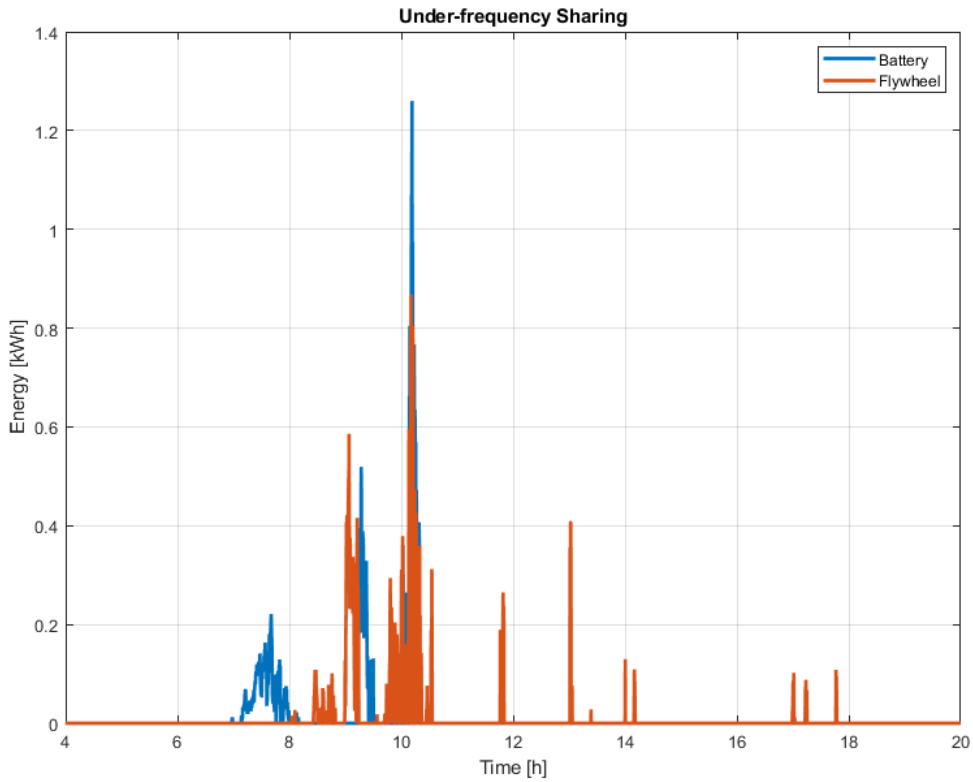


Figure 49: Under-frequency sharing strategy.

# 8 Project Summary

The objective of this section is to estimate the research and development cost as well as the environmental impact caused of the realization of the project and from the implementation of the solution developed.

## 8.1 Budget Estimation

Each of project phases are characterized by hour spent and a common remuneration per hour set as 10€/h.

| Human Resources Estimation | | |
|---|---|---|
| **Phase** | **Hours [h]** | **Remuneration [€]** |
| Literature Research | 75 | 750 |
| Modelling | 150 | 1500 |
| Simulation | 200 | 2000 |
| Writing | 150 | 1500 |
| **Total** | 575 | 5750 |

## 8.2 Environmental Impact

### 8.2.1 Implementation of the solution

The implementation of the HSS coupled with a PV power plant has as a direct effect on the energy system's usage of other types of generating units, thus decreasing the reliance on fossil fuel units. In fact, taking in account the carbon intensity perkilowatt-hour (CIPK) of catalan grid, is possible to quantify the positive impact of the HSS implementation analyzing the added electricity sold on the grid. The data is shown in Table 9

Table 9: Quantification of added electricity sold daily on the grid.

| Environmental Impact Estimation: Implementation | |
|---|---|
| **Scenario** | **Overall electricity sold [kWh]** |
| Base | 58 665 |
| HSS | 66 190 |
| $\Delta$ | - 7 526 |

Taking in account estimation of carbon intensity of electricity in 2018 for grid in Catalunya it is possible to estimate the avoided carbon dioxide equivalent emissions from the energy system (see Equation 59). Generalitat de Catalunya provides the value of 321 $gCO_{2eq}/kWh$ on the most recent report dedicated to climate change [49].

$$CO_{2saving} = \Delta \cdot \text{CIPK} \cdot 365 \text{ days} \cdot 15 \text{ yrs} = 13.22 \cdot 10^6 \text{ kgCO}_{2eq} \tag{59}$$

### 8.2.2 Realization of the Project

This section analyzes the environmental impact produced by the realisation of this project. Two main emission sources are identified: electrical device, namely laptop, and the thermal unit for AC service. Taking in account the same CIPK used for Section 8.2.1 it is quantified in Table [?] the overall emission estimation.

Table 10: Quantification of the project realization carbon footprint.

| Environmental Impact Estimation: Realization | | | |
|---|---|---|---|
| **Electrical Device** | **Hours [h]** | **Power [kW/person]** | **$CO_2eq$ [kg]** |
| Laptop | 575 | 0.085 | 15.7 |
| AC unit | 300 | 0.125 | 12.0 |
| **Total** | - | - | 27.7 |

# 9 Conclusions

The main economical output of the research is that the HSS implementation results in a higher profit for the plant owner, adding 0.122 M€ on top of 0.665 M€ undertaken as upfront cost resulting in 5.45 years of payback time.
It is important to highlight that costs accounted and expressed in Equation 20 include also for degradation costs which can be referred as a virtual cost, not truly undertaken by the plant owner. At the same time costs do not include maintenance, installation and engineering costs.

Another cost that could be taken in account is the energy requested by the flywheel not to fall under the minimum SoC level allowed. This energy has to be supplied by the grid, since no energy is available from the solar radiation at the time in which is needed. The daily amount of energy requested is 2.5 kWh. Considering on the one hand the weather variability and on the other hand the fact that the device presents a higher value of SoC at the end of the day than than from the beginning, this amount of energy can be taken as an average for the annual cost analysis. At the end of the year charging the flywheel from the grid will cost the plant owner more or less 90 €.[1] Taking in account the added revenues from HSS implementation this cost can be discarded without significative difference.

Finally, it is important to highlight that great part of the added revenues in the Linear Scenario are supplied not by the variable compensation (dependant from the actual energy delivered for FCR) but from the availability window, that depend finally from the bid power $P_{bid}$ and $h_{bid}$.

## 9.1 Future work

**PVPP Size**

As a first future step, it could be investigated the result of the HSS implementation coupled with smaller sized PVPPs. The effect of such a choice are:

1. Lower energy needed for PFC: since the power capacity is decreased, also the absolute value of energy requested for frequency deviations;

2. Higher variation in Power output: for the purpose of this study the 9.4 MW PVPP was modeled

[1] For the calculation it was considered the average price in 2018 for utilities in Spain [50].

as a low-pass filter. This simplification no longer applies when the area of the plant is reduced.

While the first effect could represent a loss in terms of the economical revenues (even if in a marginal way, as described previously), the second could improve the case with no battery because of the ramp rate control. In fact, for the case studied, practically no time instant suffered from ramp rate control curtailment, meaning that the effect of the plant size reduced the variability of power output.
If the variability increases, curtailment using PV inverter could lower furtherly the revenues from base case scenario. In this case, the implementation of the HSS could improve even more the economic positive benefit of the HSS installation.

**Prediction**

The method proposed for PV power output prediction focuses on the error minimization of the hourly energy sold on the DAM. On the other hand, as previously discussed in Section 5.3.2, a higher quality forecast is key in order to limit losses.

As a future work step it can be implemented a more accurate predictive method, implementing statistical approach such as Artificial Neural Networks models [51]. A better forecast prediction could decrease the need for storage lowering forecasting error for DAM scheduling.

**Quadratic Degradation Scenario**

Finally, more accurate quadratic degradation cost should be applied as in Equation 3 to the GAMS model. The difficulty faced by the author has been mainly computation requirements: it was more strategic for the project management and thesis outcome to use linear degradation scenario output and to proceed with simulation evaluation than to obtain more accurate input data from GAMS optimization.

**Sensitivity Analysis**

As a future step it could be assessed the viability of the power reserve service for more than one day, given different set of irradiance data, for different weather and seasonal conditions. The thesis work focused only on one reference day (01.04.2019) that can be taken as a reference for the month of April, but the author proposes as a further step a monthly assessment throughout the year:

- Given the setup selected, is the HSS capable of providing the FCR service each month?
- If the service cannot be ensured during certain days, the electricity to charge the battery can be bought from the grid. How is this strategy affecting the profitability of the project?

- Given the results throughout the year, what is the number of daily hours bid in the Reserve market that ensures the global maximum during the entire year?

**Post-processing Rainflow Algorithm**

Finally, the added economical value of the implementation of the flywheel should be quantified highlighting in post-processing phase the reduced stress on the battery implementing the hybrid solution compared to a no-flywheel scenario (as developed in [14]).

# 10 Matlab Codes

## 10.1 Voltage Controller

```
function y = fcn(time, i, imax, SoC, minSoC, BUfr)
if time<2400 || time > 3360 %starting bid time instant and end bid time instant
    y = i;
else
    if BUfr >0
        y=0;
    else
        if SoC <= minSoC
            y = 0.1*imax;
        else
            if i<-0.1*imax
            y=-0.1*imax;
            else
                if i>0.1*imax
                y=0.1*imax;
                else
                y=i;
            end
        end
    end
end
end
end
```

## 10.2 Torque Control

```
function Tstar = fcn(T,SoC)

if T>=0
```

```
    if SoC>=1.0
        Tstar=0;
    else
        Tstar=T;
    end
else
    if SoC<=0.15
        Tstar=0;
    else
        Tstar=T;
    end
end
```

## 10.3 Over-frequency Control

```
function [Ebat,Efly,EPv] = OFRcontrol(BCap,BSoC,ofr,FSoC,FCap)
        if FSoC + ofr <= FCap
            Efly = ofr;
            Ebat = 0;
            EPv = 0;
        else
            if BSoC + ofr <= BCap
                Efly=0;
                Ebat=ofr;
                EPv = 0;
            else
                Efly = 0;
                Ebat = 0;
                EPv = ofr;
            end
        end
end
```

## 10.4 Under-frequency Control

```
function [Ebat,Efly] = UFR(t,UFR,FSoC)
    if (2400<=t)&&(t<=3660)
        if FSoC >= 0.5
            Efly = UFR;
            Ebat =0;
        else
            Efly=0;
            Ebat=UFR;
        end
    else
        Ebat =0;
        Efly = UFR;
    end
end
```

## Acknowledgments

I would like to thank first of all my grandfathers: Nonna Angela, you are my symbol of humility, strength and wonderful simplicity. You have been through difficult times for decades, never loosing your beautiful independence of Woman. Thank you for making my Sundays every time more cheerful.

Nonno Giuseppe you are reading everyday at the age of 89 years old, making of yourself a living demonstration that learning is a never ending process, no matter where you start from. Your love for politics is an example, your active and spontaneous commitment for society is a call of individual duty.

Nonna Laura you are the sweet symbol of my Mediterranean roots: always smiling, always sharing and always kind.

Thank you to all my family, especially my father for supporting every confused and undefined step I take towards my academical, professional and human life.

A big thank you to my supervisor Francisco for having the immense patience to listen to all of my questions.

My roomies, my friends, Fridays for Future and all who made this experience in Barcelona a meaningful experience.

## References

[1] Debra Roberts, Roz Pidcock, Yang Chen, Sarah Connors, and Melinda Tignor. Global Warming 1.5 C. pages 1–630, 2018.

[2] Gates Bill. Climate change and the 75% problem | Bill Gates, 2018.

[3] Energy Watch Group. *Global Energy System based on 100% Renewable Energy Energy Transition in Europe Across Power, Heat, Transport and Desalination Sectors*. Number April. 2019.

[4] IRENA. *Renewable-Powered Future : Solutions To Integrate*. 2019.

[5] Carlos Galilea. Economic analysis of residential PV self-consumption systems with Li-ion batteries under different billing scenarios. *2019 IEEE International Conference on Environment and Electrical Engineering and 2019 IEEE Industrial and Commercial Power Systems Europe (EEEIC / I*, page 1, 2019.

[6] Benedikt Battke and Tobias S. Schmidt. Cost-efficient demand-pull policies for multi-purpose technologies – The case of stationary electricity storage. *Applied Energy*, 155:334–348, oct 2015.

[7] K. Prompinit and S. Khomfoi. Ramp rate consideration of a BESS using active power control for PV generation. *2015 18th International Conference on Electrical Machines and Systems, ICEMS 2015*, pages 1676–1680, 2016.

[8] Guishi Wang, Mihai Ciobotaru, and Vassilios G. Agelidis. Optimal capacity design for hybrid energy storage system supporting dispatch of large-scale photovoltaic power plant. *Journal of Energy Storage*, 3:25–35, 2015.

[9] Matthias Resch. *Large Scale Battery Systems in Distribution Grids*. PhD thesis, 2018.

[10] Dennis Metz and João Tomé Saraiva. Use of battery storage systems for price arbitrage operations in the 15- and 60-min German intraday markets. *Electric Power Systems Research*, 160:27–36, 2018.

[11] Iain Staffell and Mazda Rustomji. Maximising the value of electricity storage. *Journal of Energy Storage*, 8:212–225, 2016.

[12] Ye Yang, Qing Ye, Leonard J. Tung, Michael Greenleaf, and Hui Li. Integrated Size and Energy

Management Design of Battery Storage to Enhance Grid Integration of Large-Scale PV Power Plants. *IEEE Transactions on Industrial Electronics*, 65(1):394–402, 2018.

[13] Guishi Wang, Student Member, Mihai Ciobotaru, Vassilios G Agelidis, and Senior Member. Power Smoothing of Large Solar PV Plant Using. *Ieee*, 9:1–9, 2014.

[14] L. Barelli, G. Bidini, F. Bonucci, L. Castellini, A. Fratini, F. Gallorini, and A. Zuccari. *Flywheel hybridization to improve battery life in energy storage systems coupled to RES plants*. Elsevier B.V., 2019.

[15] Cristina Vitale and Francisco Diaz-Gonzalez. Optimization of PV power plant operation through energy storage providing ancillary services REPORT Author: Escola Tècnica Superior d'Enginyeria Industrial de Barcelona. Technical report, 2018.

[16] Bolun Xu, Jinye Zhao, Tongxin Zheng, Eugene Litvinov, and Daniel S. Kirschen. Factoring the Cycle Aging Cost of Batteries Participating in Electricity Markets. *IEEE Transactions on Power Systems*, 33(2):2248–2259, 2018.

[17] EUETS. Frequency Containment Reserve (FCR).

[18] EUETS. European Union Electricity Market Glossary - Frequency Restoration Reserve (FRR).

[19] F. Bignucolo, R. Caldon, M. Pettinà, and F. Pasut. Renewables contributing to Primary Control Reserve: The role of Battery Energy Storage Systems. *Conference Proceedings - 2017 17th IEEE International Conference on Environment and Electrical Engineering and 2017 1st IEEE Industrial and Commercial Power Systems Europe, EEEIC / I and CPS Europe 2017*, pages 1–6, 2017.

[20] Francisco Díaz-González, Melanie Hau, Andreas Sumper, and Oriol Gomis-Bellmunt. Participation of wind power plants in system frequency control: Review of grid code requirements and control methods. *Renewable and Sustainable Energy Reviews*, 34:551–564, 2014.

[21] REE Red Eléctrica de España. Operation of the electricity system | Red Eléctrica de España.

[22] José Pablo Chaves-Ávila. European Short-term Electricity Market Designs under High Penetration of Wind Power, 2014.

[23] Leon Maximilian Haupt. Centralised Battery Flexibility Assessment for Imbalance Management

in Spain considering Li-Ion Degradation Mechanism. page 166, 2018.

[24] National Grid ESO. Historic frequency data | National Grid ESO.

[25] National Grid ESO. Post Tender Report -TR111 March 2019 - EXT. 2019.

[26] Antonio Gomez Exposito and Antoni Sudria i Andreu. *El almacenamiento de energia en la distribucion electrica del futuro*. Real Academia de Ingenieria, Madrid, 2017.

[27] Matthias Resch, Jochen Bühler, Birgit Schachler, Rita Kunert, Andreas Meier, and Andreas Sumper. Technical and economic comparison of grid supportive vanadium redox flow batteries for primary control reserve and community electricity storage in Germany. *International Journal of Energy Research*, 43(1):337–357, jan 2019.

[28] B. Dunn, H. Kamath, and J.-M. Tarascon. Electrical Energy Storage for the Grid: A Battery of Choices. *Science*, 334(6058):928–935, nov 2011.

[29] Francisco. Diaz-Gonzalez, Andreas. Sumper, and Oriol. Gomis-Bellmunt. *Energy storage in power systems*.

[30] Todd C. Frankel. Cobalt mining for lithium ion batteries has a high human cost - Washington Post.

[31] Beacon Power LCC. Beacon Power Flywheel Energy Storage Systems. Technical report.

[32] Mustafa E. Amiryar and Keith R. Pullen. A review of flywheel energy storage system technologies and their applications. *Applied Sciences*, 7(3), 2017.

[33] R. Sebastián and R. Peña Alzola. Flywheel energy storage systems: Review and simulation for an isolated wind power system. *Renewable and Sustainable Energy Reviews*, 16(9):6803–6813, 2012.

[34] Rickard Östergård. Flywheel energy storage - a conceptual study. *Uppsala Universitet*, 48(December):1–48, 2011.

[35] Timm Weitzel, Maximilian Schneider, Christoph H. Glock, Florian Löber, and Stephan Rinderknecht. Operating a storage-augmented hybrid microgrid considering battery aging costs. *Journal of Cleaner Production*, 188:638–654, 2018.

[36] E. Sarasketa-Zabala, I. Gandiaga, E. Martinez-Laserna, L. M. Rodriguez-Martinez, and I. Villarreal. Cycle ageing analysis of a LiFePO4/graphite cell with dynamic model validations: Towards realistic lifetime predictions. *Journal of Power Sources*, 275:573–587, 2015.

[37] Stig Odegaard Ottesen, Pol Olivella-Rossell, Pau Lloret, and Ari Hentunen. Invade Project D5.3 Simplified Battery operation and control algorithm. (731148), 2017.

[38] Madeleine Ecker, Nerea Nieto, Stefan Käbitz, Johannes Schmalstieg, Holger Blanke, Alexander Warnecke, and Dirk Uwe Sauer. Calendar and cycle life study of Li(NiMnCo)O2-based 18650 lithium-ion batteries. *Journal of Power Sources*, 248:839–851, 2014.

[39] Evelina Wikner and Evelina Wikner. *Ageing in Commercial Li-ion Batteries : Lifetime Testing and Modelling for Electrified Vehicle Applications*. 2019.

[40] IRENA. *Electricity storage and renewables: Costs and markets to 2030*. Number October. 2017.

[41] Eduard Bullich-Massagué, Mònica Aragüés-Peñalba, Andreas Sumper, and Oriol Boix-Aragones. Active power control in a hybrid PV-storage power plant for frequency support. *Solar Energy*, 144:49–62, 2017.

[42] MIDC. MIDC: Oahu Solar Measurement Grid.

[43] Dennis J Coyle, Holly A Blaydes, Rebecca S Northey, James E Pickett, Kaustubh R Nagarkar, Rian Zhao, and James O Gardner. From irradiance to output power fluctuations: the pv plant as a low pass filter. *Progress in Photovoltaics*, (October 2011):156–172, 2013.

[44] Anna Mayo Palau. Dimensionat de bateries d'un parc fotovoltaic per a la reducció de costos en els errors de predicció. Technical report.

[45] E-sios REE Red Eléctrica de España. Bienvenido | ESIOS electricidad · datos · transparencia.

[46] Lewis Johnston, Francisco Díaz-González, Oriol Gomis-Bellmunt, Cristina Corchero-García, and Miguel Cruz-Zambrano. Methodology for the economic optimisation of energy storage systems for frequency support in wind power plants. *Applied Energy*, 137:660–669, jan 2015.

[47] Milos Hauskrecht. Linear Regression. *Regression Methods in Biostatistics*, pages 69–131, 2005.

[48] Luis Galván, Juan M. Navarro, Eduardo Galván, Juan M. Carrasco, and Andrés Alcántara. Opti-

mal scheduling of energy storage using a new priority-based smart grid control method. *Energies*, 12(4), 2019.

[49] Generalitat Catalunya. Guia pràctica per al càlcul d'emissions de gasos amb efecte d'hivernacle (GEH) 0 GUIA PRÀCTICA PER AL CÀLCUL D'EMISSIONS DE GASOS AMB EFECTE D'HIVERNACLE (GEH). Technical report.

[50] Fernando Forte. • Industry prices for electricity in Spain 2008-2018 | Statista.

[51] Cyril Voyant, Gilles Notton, Soteris Kalogirou, Marie-Laure Nivet, Christophe Paoli, Fabrice Motte, and Alexis Fouilloy. Machine learning methods for solar radiation forecasting: A review. *Renewable Energy*, 105:569–582, may 2017.